



Published in final edited form as:

Sci Transl Med. 2025 January 08; 17(780): eadk8623. doi:10.1126/scitranslmed.adk8623.

Hypoxia-inducible factor 2 regulates alveolar regeneration after repetitive injury in three-dimensional cellular and in vivo models

A. Scott McCall¹, Sergey Gutor², Hari Tanjore¹, Ankita Burman^{1,3}, Taylor Sherrill¹, Micah Chapman¹, Carla L. Calvi¹, David Han¹, Jane Camarata¹, Raphael P. Hunt¹, David Nichols¹, Nicholas E. Banovich⁴, William E. Lawson^{1,5}, Jason J. Gokey¹, Jonathan A. Kropski^{*,1,4,5,6}, Timothy S. Blackwell^{*,1,2}

¹Division of Allergy, Pulmonary and Critical Care Medicine, Department of Medicine, Vanderbilt University Medical Center, Nashville, TN 37232

²Department of Internal Medicine, University of Michigan Medical School, 48109

³University Health Network, Toronto Lung Transplant Program, Toronto, Ontario, Canada, M5G 2N2

⁴Translational Genomics Research Institute, Phoenix, AZ, 85004

⁵Department of Veterans Affairs Medical Center, Nashville, TN, 37212

⁶Department of Cell and Developmental Biology, Vanderbilt University School of Medicine, Nashville, TN 37232

Abstract

Idiopathic pulmonary fibrosis (IPF) is a progressive interstitial lung disease in which repetitive epithelial injury and incomplete alveolar repair result in accumulation of pro-fibrotic intermediate/transitional “aberrant” epithelial cell states. The mechanisms leading to the emergence and persistence of aberrant epithelial populations in the distal lung remain incompletely understood. By interrogating single-cell RNA sequencing (scRNA-seq) data from patients with IPF and a mouse model of repeated lung epithelial injury, we identified persistent activation of hypoxia-

Corresponding authors: Timothy S. Blackwell (timblack@umed.mich.edu) and Jonathan A. Kropski (jon.kropski@vumc.org).

*denotes equal contribution

Author contributions:

Conceptualization: ASM, WEL, JAK, TSB

Formal Analysis: ASM, NEB, JAK

Data curation: JAK

Methodology: ASM, SG, HT, AB, MC, CLC, DN, NEB, JG, JAK, TSB

Investigation: ASM, SG, HT, AB, TS, MC, DH, JC, RPH, DN,

Visualization: ASM

Writing (Lead): ASM

Writing – Review and Editing: AB, NEB, JG

Writing – Original Draft Preparation: JAK, TSB

Funding Acquisition: JAK, TSB

Supervision: JAK, TSB

List of Supplementary Materials

Supplementary Materials and Methods

Figures S1 to S13.

Tables S1 to S3.

Data files S1 and S2.

References (75–89)

inducible factor (HIF) signaling in these aberrant epithelial cells. Using mouse genetic lineage-tracing strategies together with scRNA-seq data, we found that these disease-emergent aberrant epithelial cells predominantly arose from airway-derived (*Scgb1a1-CreER*-traced) progenitors and exhibited transcriptional programs of *Hif2a* activation. In mice treated with repetitive intratracheal bleomycin, deletion of *Epas1* [Hif2a] but not *Hif1a*, from airway-derived progenitors, or administration of the small-molecule HIF2 inhibitor PT-2385, using both prevention and rescue approaches, attenuated experimental lung fibrosis, reduced the appearance of aberrant epithelial cells, and promoted alveolar repair. In mouse alveolar organoids, genetic or pharmacologic inhibition of Hif2 promoted alveolar differentiation of airway-derived epithelial progenitors. In addition, treatment of human distal lung organoids with PT-2385 increased colony-forming efficiency, enhanced protein and transcriptional markers of alveolar type 2 epithelial cell maturation, and prevented the emergence of aberrant epithelial cells. Together, these studies showed that HIF2 activation drives the emergence of aberrant epithelial populations after repetitive injury and that targeted HIF2-inhibition may represent an effective therapeutic strategy to promote functional alveolar repair in IPF and other interstitial lung diseases.

One sentence summary:

Inhibiting hypoxia-inducible factor 2 promotes functional alveolar epithelial repair following recurrent lung injury.

Introduction

Despite the development and widespread utilization of first-generation antifibrotic therapies (1, 2), the morbidity and mortality of idiopathic pulmonary fibrosis (IPF) remains high with median survival of 3–5 years after diagnosis (3), underscoring a substantial unmet need for improved disease-modifying treatments. Genetic and genome-wide association studies have linked epithelial-restricted genes (including *SFTPC* [*Surfactant protein-C*], *MUC5B* [*Mucin 5B*], *DSP* [*Desmoplakin*] and others) to IPF risk (4–6), supporting a conceptual model of IPF pathogenesis wherein the disease develops as a result of repetitive or chronic lung epithelial injury with a dysregulated repair process (7, 8). Single-cell transcriptomic studies have revealed extensive changes in molecular programs of epithelial cells in IPF, resulting in the emergence and persistence of multiple intermediate and transitional states within the distal airway and alveolar niches (9, 10), including *KRT5* [Keratin 5]⁻ *KRT17* [Keratin 17]⁺ *P63* [Tumor Protein 63]⁺ “aberrant basaloid” cells (11–13). These findings highlight the need to better understand the molecular mechanisms that underlie dysregulated epithelial homeostasis and repair in IPF.

The fundamental role of the lung epithelium is to interact with the external environment and maintain the barrier for gas exchange. In the alveolar niche, alveolar type 2 (AT2) serve as a facultative stem cell, self-renewing and giving rise to new alveolar type 1 (AT1) cells during lung regeneration (14). Multiple groups have now identified both homeostatic and disease-emergent cell types/states with expression of genes that serve as distal-airway markers (*SCGB3A2* [*Secretoglobin 3A2*], *SFTPB* [*Surfactant Protein B*]) that may contribute to “attempted” alveolar repair in IPF (11) and other chronic lung diseases (9, 15, 16); these cells share some features with injury-emergent transitional states observed in mouse models

(10, 17, 18). Some of these cells can give rise to mature AT2 cells in vitro and likely represent an additional stem-cell reservoir being tapped to regenerate the alveolar niche (9, 15). Although the relative contributions of resident AT2 cells and distal airway derived stem cells [including respiratory airway secretory cells (RASCs) (15), terminal-airway secretory cells (TASCs) (16) or terminal respiratory bronchiole secretory cells (TR-BSC) (9)] in repopulating injured alveoli in the context of IPF remain uncertain, factors governing the response of each of these populations to repetitive injury are likely key determinants of adaptive versus maladaptive repair.

In the lung epithelium, the Hypoxia-inducible factor (HIF) family of transcription factors has previously been implicated as a determinant of airway epithelial repair following influenza infection (18) and can facilitate development of a mucus-secretory cell phenotype (19, 20). In addition, HIF activation in endothelial cells underlies vascular remodeling in pulmonary hypertension (21, 22). However, a role for HIF signaling in lung fibrosis has not previously been established (23). HIF activation can occur via two distinct but not exclusive mechanisms: i) inhibition of prolyl-hydroxylases when oxygen tension is low, and ii) through changes in cell redox state, which can be influenced by inflammatory signaling, glycolytic tone, or other oxidative metabolism or enzymatic activities (24). Tonic degradation of HIF α (both HIF1 α and HIF2 α [Endothelial PAS domain protein 1, *EPAS1*]) is accomplished through proline hydroxylation and subsequent poly-ubiquitination by the Von-Hippel-Lindau (VHL) complex. Under activating conditions, HIF1 (or HIF2) α escapes degradation, binds HIF1 β (Aryl Hydrocarbon Nuclear Translocator, ARNT), and is transported to the nucleus where it binds to genes containing a HRE (Hypoxia Response Element) to enhance transcription. Despite recognizing identical consensus sequences, HIF1 α and HIF2 α exhibit unique, non-competitive transcriptional regulatory programs (25), and also display different activation kinetics (26) with HIF2 α demonstrating more prolonged transcriptional activity under chronic activation (19).

Using epithelial-targeted Hif deficient mice paired with single-cell RNA sequencing (scRNA-seq), we observed that both AT2 and airway secretory cells contribute to alveolar repair following repetitive bleomycin injury. Combined deletion of Hif1 and Hif2 in the lung epithelium attenuated fibrosis and promoted cellular programs associated with alveolar repair and maturation. Using cell-type-specific conditional deletion strategies, we established that this protection was mediated primarily by Hif2-deletion in airway-derived progenitors. Targeted pharmacologic HIF2 inhibition with PT-2385 (a selective HIF2 α : HIF1 β dimerization inhibitor) enhanced alveolar repair and differentiation of airway-derived cell populations in mice even when initiated after fibrosis was established. In addition, ex-vivo studies showed HIF2-inhibition promoted distal airway to alveolar differentiation. Human distal lung organoid cultures revealed enhanced proliferation and suppression of aberrant transitional cell states closely resembling IPF-emergent epithelial cell states. Together, these results indicate that HIF2 is a key regulator of distal lung epithelial repair and suggest HIF2 inhibition as a therapeutic strategy for enhancing lung regeneration.

Results

To investigate the cellular mechanisms that underlie epithelial dysregulation in IPF, we interrogated our previously published scRNA-seq dataset generated from 67 pulmonary fibrosis (PF) and 49 control (declined donor) lungs (20) (Fig. 1A–B). Focusing on the KRT5⁺KRT17⁺ “aberrant-basaloid” cells that emerge in IPF lungs and exhibit profibrotic gene expression profiles (11, 12), we performed a pathway and transcription factor analysis of genes with Log₂FC >1. In addition to several pathways that have been previously described in these cells (epithelial-mesenchymal transition, p53, tumor-necrosis alpha signaling) (Fig. 1C), transcription factor coexpression analysis revealed significant enrichment of both *HIF1A* ($p=4.7 \times 10^{-49}$) and *EPAS1* ($p=2.93 \times 10^{-8}$) regulated genes, and a “hypoxia module” (comprised of identified HIF-regulated genes) was also significantly higher in IPF-derived cells compared to controls (Fig. 1D) ($p < 2 \times 10^{-16}$). This suggested that HIF signaling may be a driver of aberrant epithelial cell phenotypes in PF.

To examine the mechanisms that underlie resolving versus non-resolving lung fibrosis in mice, we challenged C57B6 mice with a single dose of intratracheal (IT) bleomycin (SD Bleo, 0.08 IU) or repeated biweekly IT bleomycin (Rep Bleo, 0.04 IU) and sacrificed mice 14 days after the last bleomycin dose (Fig. 1E). Compared to the lungs of unchallenged mice (Fig. 1F(a–c)), the lungs of mice treated with SD Bleo contained inflammatory infiltrates and patchy fibrosis (Fig. 1G(a–c)), whereas the lungs of mice treated with Rep Bleo exhibited discrete areas of epithelial hyperplasia in the parenchyma (resembling microscopic honeycombing) along with interalveolar septal thickening and fibrosis (Fig. 1H(a–c)). To define the cellular and molecular programs following acute versus repeated injury, we performed scRNA-seq of Cd326⁺ (Epcam)-sorted epithelial cells (n=3 mice per group). In addition to canonical lineages (AT1, AT2, MCC [Multiciliated], PNEC [pulmonary neuroendocrine cells]), we observed a number of injury-emergent cell types/states, including *Krt5*⁺*Trp63*⁺ basal-like cells, *Muc5b* [*Mucin 5b*]⁺ secretory cells, airway *Sox2* [*Sry-box transcription factor 2*]⁺ and alveolar (*Krt8* [*Keratin 8*]⁺ *Cdkn1a* [*Cyclin-dependent kinase inhibitor 1a*]⁺) intermediate cell populations, bronchio-alveolar stem-cell (BASC)-like cells (*Scgb1a1* [*Secretoglobin 1a1*]⁺/*Sftpc*⁺) (21–23), and *Sox8* [*Sry-box transcription factor 8*]⁺ microfold-like cells (24) (Fig. 1I–K, fig. S1). Compared to the SD Bleo group, lungs from Rep Bleo mice had expansion of injury-related populations including alveolar intermediate (*Krt8*⁺*Cdkn1a*⁺), BASC-like cells, and Secretory-Muc5b⁺ cells, as well as substantially reduced AT2 cells (Fig. 1L). Epithelial cells from mice treated with Rep Bleo showed higher expression of hypoxia regulated genes compared to unchallenged mice and SD Bleo-treated mice (Mouse Hallmark MsigDB hypoxia gene set, $p < 2 \times 10^{-16}$) (Fig. 1M). *Epas1* was more highly expressed in AT2, secretory, and BASC-like populations (25) (Fig. 1N and fig. S2).

Although we previously showed that lung epithelial-specific deletion of *Hif1a* and *Epas1* did not impact fibrosis in the single-dose bleomycin model (26), these results suggested that epithelial Hif activation is more prominent after chronic or recurrent injury. Given the potential for at least partial functional redundancy between Hif forms (27, 28), we then investigated the role of Hif signaling in recurrent epithelial injury by deleting both *Hif1a* and *Epas1* in mice. Lung epithelial-specific Hif1/2 deficient mice were generated using the constitutive *Sftpc-Cre* (29), referred to as Hif1/2^{epi} (26), both Hif1/2^{epi} and Cre-negative

littermate control mice were challenged with Rep Bleo (26, 30), and lungs were harvested 2 weeks after the final bleomycin dose (Fig. 2A and fig. S3). Compared to littermate controls, lungs from Rep Bleo-treated Hif1/2^{epi} mice had less architectural remodeling, reduced fibrotic area, smaller lung area occupied by hyperplastic epithelial cells, and lower collagen content (Fig. 2B–E). Building on our findings (26), these data indicated that HIF signaling impacts non-resolving lung fibrosis induced by chronic or repetitive injury.

To investigate the mechanism through which Hif deletion protects against experimental lung fibrosis following repetitive injury, we performed scRNA-seq of Cd326⁺-sorted epithelial cells from unchallenged and Rep Bleo-treated Hif1/2^{epi} and wild type (WT) mice (Fig. 2F–H). Although there were no compositional differences between unchallenged Hif1/2^{epi} mice and WT controls, after Rep Bleo injury, Hif1/2^{epi} lungs contained a larger proportion of AT2 cells (38.6% vs 22.3%) and alveolar intermediate cells (13.9 vs 7.9%), and a smaller proportion Secretory-Muc5b⁺ cells (1.0% vs 2.5%) compared to Rep Bleo-treated WT control mice (Fig. 2H). The increased frequency of distal lung cell types (AT1, AT2, Alveolar intermediate, BASC-like), suppression of PNECs, and rebalancing of the airway populations indicated broad Hif-regulated effects on epithelial population dynamics during repair after recurrent injury. RNA-in situ hybridization/Immunofluorescence for *Muc5b* and *Scgb1a1* confirmed attenuation of *Muc5b* expression within (Fig. 2I–J), and outside of conducting airways (Fig. 2K), consistent with a direct role of Hif regulation of mucous-secretory cell polarization (31).

We then examined gene-coexpression modules in airway-type cells to understand differential transcriptional program changes related to Hif-driven signaling. Using CEMiTool (32) we identified eight modules, seven of which showed significant genotype-specific enrichment (Fig. 2L, fig. S4, Data file S1). Modules 2, 4, and 5 (M2/4/5) were most strongly enriched in Hif1/2^{epi} mice after Rep Bleo treatment and demonstrated gene co-expression hubs suggesting trans-differentiation of secretory cells toward alveolar fate (*Sftpc*, *Etv5* [*ETS variant transcription factor 5*], *Lamp3* [*Lysosomal associated membrane protein 3*]). M4 in particular showed key hubs associated with 14–3–3 signaling (*Ywhae-14-3-3 epsilon*) potentially modulating *Yap* [*Yes-associated protein*] / *Taz* [*WW Domain Containing Transcriptional Regulator 1*] mediated activity (33) and *Fgfr2* [*Fibroblast growth factor receptor 2*]. Module 2 (M2) contained multiple hubs associated with airway homeostasis and disease modification [such as *MECOM* [*MDS1 and EVI1 complex locus*] in COPD (34), *ALCAM* [*Activated leukocyte cell adhesion molecule*] in IPF(39)]. Further, protein-protein interaction analysis of M2 (enriched with Hif-deletion) identified Wingless (Wnt)-signaling hubs (Glycogen-synthase kinase 3 β , Gsk3 β) and the transcriptional repressor of the notch pathway *Atxn1* [*Ataxin 1*] (35), further supporting the role of Hif-signaling and its interaction with the Wnt/Notch axis with distal lung repair during injury (19). These findings positioned Hif-activation as an upstream inhibitor of airway to alveolar epithelial cell transition and were further supported by the enhancement of the AT2-like program within M5 containing protein-protein hubs *Cepba* [*CCAAT enhancer-binding protein alpha*] and *Lrrk2* [*Leucine-rich repeat kinase 2*] (fig. S5). Module 6 was highly enriched in wild-type (WT) cells and aligned with airway cell phenotypes, including *Scgb3a1* [*Secretoglobin 3a1*], *Muc5b*, the transcription factor *Ltf* [*Lactoferrin*] and known Hif-responsive gene *Scnn1b* [*Sodium channel epithelial 1 subunit beta*], a pattern also seen with the other

hypoxic-signaling changes reported recently regarding specific secretory populations (31, 36). Pathway analysis of the Hif1/2^{epi}-enriched modules showed associations with proliferation, secretory function, and biosynthetic machinery associated with cholesterol and lipid synthesis (Fig. 2L). These data cumulatively suggested that deletion of *Hif* specifically in lung epithelial cells enables improved adaptive repair through modulation of underlying transcriptional programs with resultant decreases in mucous secretory cell and increases in BASC-like and secretory cell programs.

To establish the origins of Hif-activated epithelial cells that emerge following recurrent injury, we performed lineage-tracing studies using tamoxifen-inducible *Sftpc-Cre-ER^{T2}* (AT2-specific) and *Scgb1a1-Cre-ER^{T2}* (secretory cell-specific) tDtomato reporter mice (Fig. 3A). After administration of tamoxifen followed by >3-week washout, mice were treated with 4 cycles of Rep Bleo treatment, and CD326⁺/dTomato⁺ cells were sorted by FACS for scRNA-seq (Fig. 3B–C). Compositional analyses revealed that the *Scgb1a1*-derived population, as opposed to the *Sftpc*-derived population, resembled the spectrum of epithelial cell phenotypes recovered following a pan-epithelial sort from mice following chronic injury (MCC, AT2, Alveolar intermediate, and BASC-like cells), suggesting these *Scgb1a1*-lineage labeled cells were substantial contributors to repair of recurrent epithelial injury (Fig. 3D) consistent with other recent dual-recombinase-based cell fate mapping studies (37). Using pimonidazole (Pim) to detect intracellular hypoxia-related reductive species (38), we observed that in unchallenged mice, there were negligible Pim⁺ cells, whereas abundant Pim⁺ Scgb1a1-traced cells were observed in both the airway and in the repairing parenchyma in Rep Bleo-treated mice, including patches of Spc⁺Scgb1a1⁺Pim⁺ cells within areas of parenchymal remodeling, supporting the concept of Hif-driven modulation of repair within this population (Fig. 3E). Consistent with our initial transcriptomic studies (Fig. 1L), we identified nuclear-localized (active) Hif2 α protein and numerous dTom⁺Scgb1a1⁺Hif2 α ⁺ cells in the lung parenchyma of mice following Rep Bleo, whereas Hif1 α ⁺ cells were limited to the proximal airways (Fig. 3F, fig. S6A–B).

We then performed conditional *Hif1a* or *Epas1* deletion studies using *Sftpc-Cre-ER^{T2}* (AT2-specific) or *Scgb1a1-Cre-ER^{T2}* (secretory cell-specific) mice. After administration of tamoxifen followed by >3-week washout, mice underwent Rep Bleo treatment. Among the four genotypes, only secretory cell-specific *Epas1*-deletion significantly protected from fibrosis (p=0.033) (Fig. 3G–H). Together, these data indicated that secretory cells act as critical facultative progenitors in repair of chronic injury and support the concept that Hif2 α activation in this cell population drives maladaptive repair.

Next, we selectively tested the role of Hif2 in regulating alveolar repair during repetitive injury by using the small molecule inhibitor (PT-2385) (39) which prevents HIF2 α :HIF1 β dimerization. In these studies, *Scgb1a1*-lineage labeled mice were challenged with biweekly repetitive IT bleomycin, and PT-2385 (6 mg/kg/day by osmotic pump) (39, 40) was initiated 7 days after the initial dose of bleomycin and continued until sacrifice at 14 days after the 6th cycle of Rep Bleo (Fig. 4A). Analysis of Hif1 and Hif2 nuclear localization demonstrated that PT-2385 appropriately suppressed nuclear localization of Hif2 (fig. S6C–D). There was a marked increase in dTomato⁺ parenchymal area in PT-2385-treated mice compared to vehicle (DMSO:propylene glycol)-treated controls (Fig. 4B–C), with

commensurate increases in the numbers and proportions of parenchymal dTomato⁺ cells expressing the mature alveolar markers pro-Spc (AT2) and/or Ager (AT1) (Fig. 4D–F). In addition, although the relative abundance of secretory populations, including Muc5b⁺ cells, remained unchanged in the airways; there were significantly fewer ectopic secretory cells (including Muc5B⁺ cells) outside of the conducting airways (p=0.003 for treatment effect) (Fig. 4G–I), similar to what was seen in mice with combined Hif1/2 genetic deletion (Fig. 2J–K). To understand whether Hif2 inhibition could also promote repair after the establishment of parenchymal remodeling and fibrosis, PT-2385 was initiated as a rescue treatment after the last of 4 doses of Rep Bleo and continued for 4 weeks. We again observed increased Scgb1a1-lineage-derived proliferation as well as more lineage-labeled AT1 (Hopx⁺) and AT2(pro-Spc⁺) cells. There were substantially fewer Hopx⁺/pro-Spc⁺ dual positive cells (“intermediate” or “transitional” cells (10, 17, 18, 41)), suggesting that Hif2 inhibition facilitated more maturation of airway progenitor-derived alveolar epithelial cells (Fig. 4J–O and fig. S6E). We also quantified lung parenchymal collagen deposition and found that there were significant decreases in collagen content (with pharmacologic Hif2-inhibition by Picrosirius red staining in both the prophylactic (p=0.0210) and rescue (p=0.0368) dosing model (fig. S7, A to F). These data supported the concept that interrupting persistent Hif2 activation in the repetitively injured lung epithelium could enhance distal lung epithelial repair and alveolar regeneration.

To determine whether the impacts of Hif2 activation were due to autonomous effects on regenerating epithelial cells, we sorted Cd326⁺/dTomato⁺ cells from naive Scgb1a1^{dTom} mice and established feeder-free alveolar organoids using “serum-free, feeder-free media” (SFFF) (42) in matrigel droplets (Fig. 5A–B). Consistent with our in-vivo findings, PT-2385-treated Scgb1a1^{dTom} derived organoids had more robust AT2-marker acquisition (pro-Spc⁺) compared to vehicle-treated controls (Fig. 5C–D), while maintaining AT1 differentiation potential (Fig. 5E–G, fig. S8A–B). We observed similar findings using genetic Hif-targeting (fig. S8C). Hif2 deletion in Scgb1a1-lineage labeled cells was associated with significantly enhanced AT2-marker acquisition, whereas the frequency of pro-Spc⁺ cells was similar in Hif1-deleted and WT organoids (p=0.0218 vs WT and p=0.0025 vs. Hif1) (Fig. 5H–J). These findings supported the concept that Hif2 activation in airway-derived repairing epithelium restrains alveolar differentiation potential, and that this can be rescued through Hif2-specific inhibition.

We then turned to a human alveolar organoid model to establish whether HIF2 also regulates alveolar progenitor potential in the human lung (Fig. 6A). Following initial expansion after isolation of CD326⁺ epithelial cells from declined lung donors under serum-free feeder-free (SFFF) conditions (9, 42), we disaggregated and re-established feeder-free organoids that were immediately treated with 20μM PT-2385 or vehicle (DMSO). Pro-SPC⁺, SCGB3A2⁺ and KRT8⁺ cells could be found within the same organoid, suggesting some plasticity among these cell types under these conditions which was also further explored by scRNA-seq (Fig. S9A–C). By day 14, PT-2385-treated organoids were more abundant (Fig. 6B–C) and demonstrated robust lysotracker staining (indicating lysosomal-related organelles associated with surfactant production) (43), results we confirmed using primary distal lung epithelial cells from IPF lungs (Fig. S10A–B).

We next analyzed scRNA-seq of Vehicle and PT-2385 organoids which demonstrated seven cell-types/states, including AT2, RASC-AT2 (*SCGB3A2*⁺*SFTPC*⁺) states, along with other activated/intermediate states (Fig. 6D–H, S9B–C). A unique population of “Aberrant intermediate” cells was less frequently observed in PT-2385 treated organoids (18.4% vs 4.4%) (Fig. 6D–G). Jaccard analysis comparing the Aberrant intermediate organoid population and cell-populations observed in the IPF lung epithelium (Fig. 1A–B) demonstrated the greatest degree of similarity ($p = 2 \times 10^{-174}$) with the highly disease-enriched (and hypoxic-module expressing) KRT5⁺KRT17⁺ cells (Fig. 6F). Pathway enrichment analysis of these Aberrant intermediate cells indicated activation of NF- κ B [Nuclear factor kappa B], which is associated with epithelial-mesenchymal transition (EMT) and maladaptive repair (44), as well as upregulation of HIF-responsive genes, including *NDRG1* [*N-myc downstream-related gene 1*], *VEGFA* [*Vascular endothelial growth factor A*], *ATF3* [*Activating transcription factor 3*], *TXNIP* [*Thioredoxin interacting protein*] which was further quantified with HIF1 and HIF2 specific gene modules (fig. S11A–D).

Although several recent reports have implicated IPF-related aberrant basal cell populations in ongoing fibrosis (45, 46), identification of transcriptional similarity with an analogous disease emergent populations from distal lung organoid culture would support the possibility that facultative stem cell populations (RASC-AT2 or AT2) are likely sources for these cell types in-vivo. mRNA-splicing-based trajectory analysis demonstrated that HIF2 inhibition led to differential dynamics, particularly between the RASC-AT2 and Aberrant intermediate clusters. Partition-based graph abstraction (PAGA)-based fate prediction suggested the RASC-AT2 to Aberrant intermediate transition was diminished by HIF2 inhibition, whereas the proliferating cell to AT2 mature and then RASC-AT2 transitions were enhanced (Fig. 6H). Further analysis using velocity kernel-based estimators predicted different terminal states and thus different quantitative dynamics for the RASC-AT2 population (Fig. S12, A to H). We observed that aberrant intermediate cells in organoids highly expressed vimentin (*VIM*) (a marker of EMT (47) and a known HIF-responsive gene (48)) both in terms of average expression and when modeled over the calculated Aberrant intermediate trajectory (Fig. 6I–J), similar to that observed in KRT5⁺KRT17⁺ in IPF (11, 12). Immunofluorescence staining revealed frequent VIM⁺ cells with nuclear (active) HIF2 in vehicle-treated organoids, which was highly suppressed by PT-2385 (Fig. 6K to M). AT1 marker acquisition following addition of differentiation media was unchanged (Fig. S13). These data collectively demonstrated that in a human distal lung organoid model, HIF2 activity regulated the phenotypic plasticity of distal lung epithelial cells, and although HIF2 activation promoted adoption of an aberrant intermediate cell state, this could be modulated by small-molecule inhibition to promote functional repair and maturation.

Discussion

Although the lung epithelium exhibits remarkable ability to repair and regenerate after acute injury, recurrent insults lead to enduring changes in the composition and molecular programs active in the lung epithelium, resulting in persistent structural remodeling and progressive decline in lung function. In this study, we found that persistent activation of HIF-signaling in repair-associated cell types/states was a hallmark of dysfunctional epithelial repair in the IPF lung epithelium and experimental models of recurrent lung epithelial injury. Further, these

dysfunctional repair-associated cell states arose primarily from airway epithelial progenitors and exhibited specific activation of HIF2. Targeted inhibition of HIF2 promoted adaptive alveolar epithelial repair and prevented fibrosis and reduced emergence of aberrant epithelial cell populations (either ectopic secretory populations or indeterminate airway-derived alveolar intermediate populations) in the distal lung which facilitated adaptive alveolar repair. Together, these findings suggest that HIF2 inhibition should be further studied as a potential therapeutic strategy to enhance lung repair in IPF and other chronic lung diseases.

Despite extensive study of facultative progenitor cell populations that participate in alveolar repair following severe acute lung injury (14, 15, 49–58), there has been limited investigation of the cellular and molecular mechanisms that regulate alveolar responses to recurrent or chronic injury. We found that recurrent epithelial injury results in mobilization of distal-airway derived progenitors, and that distal-airway-derived regeneration-associated intermediate and transitional cells with persistent activation of *Hif* and hypoxia related signaling failed to mature into functional alveolar epithelial cells. Selective inhibition of Hif2 in these regenerating airway-derived epithelial cells was sufficient to promote alveolar fate acquisition and maturation to mediate functional lung repair. Although there have been multiple characterizations of airway organoids differentiating into AT2-like Sftpc-expressing cells (55, 56, 59, 60), we observed that Hif2 inhibition markedly enhanced this cellular transition using both pharmacologic and genetic approaches.

Several studies have suggested that in the acute setting following alveolar injury, Hif1 α plays a protective role in AT2 cells (61–63). Others have also shown that Hif1 α can play a role in adaptive responses during the AT2-AT1 transition during alveolar repair (18). In contrast, Hif1 α in Sox2⁺ airway-derived progenitors attenuated lung injury following severe influenza infection along with reducing development of metaplastic Krt5⁺ “pods” via regulation of the Notch pathway (19). One potential unifying explanation for these observations is that Hif1 α plays distinct roles in specific cellular contexts, and that differences in Hif1 α kinetics influence adaptive vs. pathologic effects. There have not been previous studies of Hif2 in these contexts, and although our data indicate that Hif2 activity restrains progenitor function and alveolar fate potential while promoting airway-type metaplasia, it remains possible that Hif1 plays an additional independent or niche regulated role. One potential interpretation of the data presented here is that HIF1 α may play an adaptive, pro-survival role when transiently activated, however persistent HIF2 signaling prevents appropriate facultative progenitor function and results in dysfunctional repair. Further, it is plausible that requirements for facultative differentiation towards AT2 cells (biosynthetic burden for lipid synthesis) could be modulated through HIF2-driven metabolic changes or that HIF2 influences sensitivity to differentiation cues via modulation of the WNT/NOTCH balance (64).

Hypoxia and HIF signaling have been previously linked to mucous secretory cell differentiation (36, 65), and in this study we found that either genetic deletion of *Hif1* and *Epas1* or small-molecule-based inhibition of Hif2 was sufficient to attenuate ectopic Muc5b⁺ mucous-secretory cell differentiation. Because expansion of mucous secretory cells is a prominent feature of the IPF lung (11) and may be driven at least in part by a polymorphism in the promoter of *MUC5B* (4, 20), these findings build upon other recent work which

indicates that targeting HIF may be an effective means to ameliorate the untoward effects of mucous hypersecretion in chronic respiratory diseases while providing a tenable therapeutic target as a disease modifying agent (31).

In addition to the identification of increased mucous secretory cells, one of the most striking findings of recent single-cell transcriptomic studies has been the identification of KRT5⁻KRT17⁺ “aberrant basaloid” cells in IPF lungs (11, 12). Although questions remain as to the origin (11, 45, 66) and specific functions of these cells, a role in amplifying fibrotic signaling seems likely. We found an “Aberrant intermediate” population of cells transcriptionally resembling some features of “aberrant basaloid” cells that emerged in feeder-free culture of human distal lung epithelium (despite TGFβ [Transforming growth factor beta] inhibition), and our trajectory analyses suggested that they arose from SCG3A2⁺ “RASC-like” cells in this model; further, the emergence of these cells was largely prevented by HIF2 inhibition. Together, these results suggested a direct role for HIF2 in promoting the emergence and persistence of pro-fibrotic intermediate/transitional epithelial cell states in lung parenchyma.

These data provided evidence that activation of HIF2 is a hallmark of repetitive lung epithelial injury and can be targeted to promote distal lung repair, however there are several important limitations as well as additional questions that remain unanswered by this study. Although we observed some evidence of cellular hypoxia in areas of Hif activation, it is possible that non-hypoxic mechanisms of HIF activation are as or more important regulators of observed HIF activity in these contexts; the distinct contributions of hypoxic versus “pseudo-hypoxic” activation of HIF1 and HIF2 in distinct spatial niches were not addressed in the data presented here and will require further study. Further, it is important to note that indirect effects of HIF forms on each other via reciprocal co-regulation (for example, HIF2-mediated repression of HIF1α) (67, 68) may contribute to the observed effects on epithelial repair. These studies focused specifically on the role of HIFs in the lung epithelium, therefore it is possible that HIF2 in other cell types could also modulate overall fibrotic progression. Available data suggest the HIF family of transcription factors may also impact the function of fibroblasts (69–71), macrophages (72, 73) and the endothelium (74), which could impact the net effect of HIF targeting in IPF with other “on-target” HIF2 benefits for lung remodeling. Lastly, though we have attempted to maximally explore HIF2 inhibition in preclinical models for IPF, measurement of clinical endpoints and further human studies will be required to understand potential benefits from targeting this pathway systemically versus local administration (via nebulization) for IPF treatment. Thus, while use of PT-2385 appears promising, additional work is needed to optimize in-vivo systemic or topical dosing strategies.

In summary, we showed that recurrent injury to the distal lung and alveolar epithelium leads to persistent activation of HIF-regulated signaling in airway-derived progenitors which promotes dysfunctional epithelial repair and enhances pathological remodeling. Selective inhibition of HIF2 has the potential to enhance functional alveolar repair in patients with IPF and other chronic lung diseases.

Material and Methods

Study design:

Research Objectives: The objective of the study was to interrogate mechanisms that regulate alveolar repair of recurrent injury. *Research units of investigation* included primary cells/samples from pulmonary fibrosis and control lungs, transgenic mice, and primary cells in culture. *Experimental Design:* The experimental design was a controlled laboratory study including transcriptomic data analysis, mouse models, and organoid studies. In vitro work was performed in a minimum of three technical replicates per experimental condition and jointly analyzed where indicated. For image analysis, quantification was performed using the same cell identification and size dimension, channel positivity thresholds, and anatomical landmarks through the use of automated image analysis software (Halo, Indica Labs) established based on each immunofluorescent panel with appropriate unstained and secondary-only negative controls. Experimental and Control samples were stained from the same stock solutions and acquired under identical settings. Male and female mice were used in all experiments in as close to equivalent proportions as possible. Statistical methods are discussed in detail below; broadly non-parametric analyses were used and adjusted for multiple comparisons where appropriate. No outliers were excluded from analysis. Animals were only excluded if there was pump malfunction as detailed below, otherwise all were used in analysis. For human primary cell studies derived from declined donor samples or post-lung transplant interstitial lung disease explants, cells from both adult male and female donors were used as they became available through the duration of the work. *Blinding:* Wherever possible, data were generated and/or analyzed blinded to treatment group/genotype, use of automated and thresholded image analysis in bulk further supported impartiality.

Full detailed experimental protocols are available in the Supplementary Materials and Methods.

Statistical Analysis:

Analysis performed in this work was analyzed using a combination of GraphPad Prism v9.5.1 and R v4.3.0. All statistical tests between groups were analyzed using non-parametric methods and specified in each figure. Parametric tests, when used, are specified along with normality testing. Specific analysis parameters associated with scRNA-seq data are outlined specifically within text sections and methods along with rationale for their implementation and statistical diagnostics where applicable within the supplementary material. Except where noted for clarity, all data are plotted as median \pm 95% confidence intervals. For gene-related tests, multiple-testing adjusted p values with default settings within Seurat or scanpy were reported and used for thresholding and downstream analysis.

Supplementary Material

Refer to Web version on PubMed Central for supplementary material.

Acknowledgements

Funding:

This work was supported by NIH/NHLBI R01HL145372 (JAK/NEB), R01HL153246 (JAK), the Department of Veterans Affairs I01BX006121 (JAK), W81XWH1910415 (JAK/NEB), R01HL175555 (TSB), P01HL092870 (TSB), T32HL094296 (ASM), the Vanderbilt Faculty Research Scholars (JGG, ASM), the Pulmonary Fibrosis Foundation (ASM) and the Francis Family Foundation (JGG).

Competing interests:

JAK reports research grants/contracts from Boehringer Ingelheim and Bristol-Myers-Squibb, and consulting for APIE and ARDA. TSB reports research grants/contracts from Boehringer Ingelheim, Bristol-Myers-Squibb and Morphic. NEB reports consulting for Deepcell. The other authors report no competing interests.

Data and materials availability.

All data associated with this study are present in the paper or supplementary materials. Raw genomic data are available through the Gene Expression Omnibus (GEO) accession number GSE243252. Code for genomic analysis is available at github.com/KropskiLab/Hif_2023 and Zenodo ([10.5281/zenodo.14391160](https://doi.org/10.5281/zenodo.14391160)).

References

1. King TE Jr, Bradford WZ, Castro-Bernardini S, Fagan EA, Glaspole I, Glassberg MK, Gorina E, Hopkins PM, Kardatzke D, Lancaster L, Lederer DJ, Nathan SD, Pereira CA, Sahn SA, Sussman R, Swigris JJ, Noble PW, ASCEND Study Group A phase 3 trial of pirfenidone in patients with idiopathic pulmonary fibrosis. *N. Engl. J. Med* 370, 2083–2092 (2014). [PubMed: 24836312]
2. Richeldi L, du Bois RM, Raghu G, Azuma A, Brown KK, Costabel U, Cottin V, Flaherty KR, Hansell DM, Inoue Y, Kim DS, Kolb M, Nicholson AG, Noble PW, Selman M, Taniguchi H, Brun M, Le Maulf F, Girard M, Stowasser S, Schlenker-Herceg R, Disse B, Collard HR, INPULSIS Trial Investigators, Efficacy and safety of nintedanib in idiopathic pulmonary fibrosis. *N. Engl. J. Med* 370, 2071–2082 (2014). [PubMed: 24836310]
3. Lederer DJ, Martinez FJ, Idiopathic Pulmonary Fibrosis. *N. Engl. J. Med* 378, 1811–1823 (2018). [PubMed: 29742380]
4. Seibold MA, Wise AL, Speer MC, Steele MP, Brown KK, Loyd JE, Fingerlin TE, Zhang W, Gudmundsson G, Groshong SD, Evans CM, Garantziotis S, Adler KB, Dickey BF, du Bois RM, Yang IV, Herron A, Kervitsky D, Talbert JL, Markin C, Park J, Crews AL, Slifer SH, Auerbach S, Roy MG, Lin J, Hennessy CE, Schwarz MI, Schwartz DA, A common MUC5B promoter polymorphism and pulmonary fibrosis. *N. Engl. J. Med* 364, 1503–1512 (2011). [PubMed: 21506741]
5. Thomas AQ, Lane K, Phillips J 3rd, Prince M, Markin C, Speer M, Schwartz DA, Gaddipati R, Marney A, Johnson J, Roberts R, Haines J, Stahlman M, Loyd JE, Heterozygosity for a surfactant protein C gene mutation associated with usual interstitial pneumonitis and cellular nonspecific interstitial pneumonitis in one kindred. *Am. J. Respir. Crit. Care Med* 165, 1322–1328 (2002). [PubMed: 11991887]
6. Allen RJ, Stockwell A, Oldham JM, Guillen-Guio B, Schwartz DA, Maher TM, Flores C, Noth I, Yaspan BL, Jenkins RG, Wain LV, International IPF Genetics Consortium, Genome-wide association study across five cohorts identifies five novel loci associated with idiopathic pulmonary fibrosis. *Thorax* 77, 829–833 (2022). [PubMed: 35688625]
7. Kropski JA, Blackwell TS, Progress in Understanding and Treating Idiopathic Pulmonary Fibrosis. *Annu. Rev. Med* 70, 211–224 (2019). [PubMed: 30691371]
8. Pardo A, Selman M, Idiopathic pulmonary fibrosis: new insights in its pathogenesis. *Int. J. Biochem. Cell Biol* 34, 1534–1538 (2002). [PubMed: 12379275]

9. Kadur Lakshminarasimha Murthy P, Sontake V, Tata A, Kobayashi Y, Macadlo L, Okuda K, Conchola AS, Nakano S, Gregory S, Miller LA, Spence JR, Engelhardt JF, Boucher RC, Rock JR, Randell SH, Tata PR, Human distal lung maps and lineage hierarchies reveal a bipotent progenitor. *Nature* 604, 111–119 (2022). [PubMed: 35355018]
10. Kobayashi Y, Tata A, Konkimalla A, Katsura H, Lee RF, Ou J, Banovich NE, Kropski JA, Tata PR, Persistence of a regeneration-associated, transitional alveolar epithelial cell state in pulmonary fibrosis. *Nat. Cell Biol* (2020), doi:10.1038/s41556-020-0542-8.
11. Habermann AC, Gutierrez AJ, Bui LT, Yahn SL, Winters NI, Calvi CL, Peter L, Chung M-I, Taylor CJ, Jetter C, Raju L, Roberson J, Ding G, Wood L, Sucre JMS, Richmond BW, Serezani AP, McDonnell WJ, Mallal SB, Bacchetta MJ, Loyd JE, Shaver CM, Ware LB, Bremner R, Walia R, Blackwell TS, Banovich NE, Kropski JA, Single-cell RNA sequencing reveals profibrotic roles of distinct epithelial and mesenchymal lineages in pulmonary fibrosis. *Science Advances* 6, eaba1972 (2020). [PubMed: 32832598]
12. Adams TS, Schupp JC, Poli S, Ayaub EA, Neumark N, Ahangari F, Chu SG, Raby BA, DeJuliis G, Januszzyk M, Duan Q, Arnett HA, Siddiqui A, Washko GR, Homer R, Yan X, Rosas IO, Kaminski N, Single-cell RNA-seq reveals ectopic and aberrant lung-resident cell populations in idiopathic pulmonary fibrosis. *Science Advances* 6, eaba1983 (2020). [PubMed: 32832599]
13. Xu Y, Mizuno T, Sridharan A, Du Y, Guo M, Tang J, Wikenheiser-Brokamp KA, Perl A-KT, Funari VA, Gokey JJ, Stripp BR, Whittsett JA, Single-cell RNA sequencing identifies diverse roles of epithelial cells in idiopathic pulmonary fibrosis. *JCI Insight* 1, e90558 (2016). [PubMed: 27942595]
14. Barkauskas CE, Crouse MJ, Rackley CR, Bowie EJ, Keene DR, Stripp BR, Randell SH, Noble PW, Hogan BLM, Type 2 alveolar cells are stem cells in adult lung. *J. Clin. Invest* 123, 3025–3036 (2013). [PubMed: 23921127]
15. Basil MC, Cardenas-Diaz FL, Kathiriya JJ, Morley MP, Carl J, Brumwell AN, Katzen J, Slovick KJ, Babu A, Zhou S, Kremp MM, McCauley KB, Li S, Planer JD, Hussain SS, Liu X, Windmueller R, Ying Y, Stewart KM, Oyster M, Christie JD, Diamond JM, Engelhardt JF, Cantu E, Rowe SM, Kotton DN, Chapman HA, Morrisey EE, Human distal airways contain a multipotent secretory cell that can regenerate alveoli. *Nature* 604, 120–126 (2022). [PubMed: 35355013]
16. Rustam S, Hu Y, Mahjour SB, Rendeiro AF, Ravichandran H, Urso A, D'Ovidio F, Martinez FJ, Altorki NK, Richmond B, Polosukhin V, Kropski JA, Blackwell TS, Randell SH, Elemento O, Shaykhiiev R, A Unique Cellular Organization of Human Distal Airways and Its Disarray in Chronic Obstructive Pulmonary Disease. *Am. J. Respir. Crit. Care Med* 207, 1171–1182 (2023). [PubMed: 36796082]
17. Strunz M, Simon LM, Ansari M, Kathiriya JJ, Angelidis I, Mayr CH, Tsidiridis G, Lange M, Mattner LF, Yee M, Ogar P, Sengupta A, Kukhtevich I, Schneider R, Zhao Z, Voss C, Stoeger T, Neumann JHL, Hilgendorff A, Behr J, O'Reilly M, Lehmann M, Burgstaller G, Königshoff M, Chapman HA, Theis FJ, Schiller HB, Alveolar regeneration through a Krt8+ transitional stem cell state that persists in human lung fibrosis. *Nat. Commun* 11, 3559 (2020). [PubMed: 32678092]
18. Choi J, Park J-E, Tsagkogeorga G, Yanagita M, Koo B-K, Han N, Lee J-H, Inflammatory Signals Induce AT2 Cell-Derived Damage-Associated Transient Progenitors that Mediate Alveolar Regeneration. *Cell Stem Cell* 27, 366–382.e7 (2020). [PubMed: 32750316]
19. Xi Y, Kim T, Brumwell AN, Driver IH, Wei Y, Tan V, Jackson JR, Xu J, Lee D-K, Gotts JE, Matthay MA, Shannon JM, Chapman HA, Vaughan AE, Local lung hypoxia determines epithelial fate decisions during alveolar regeneration. *Nat. Cell Biol* 19, 904–914 (2017). [PubMed: 28737769]
20. Natri HM, Del Azodi CB, Peter L, Taylor CJ, Chugh S, Kendle R, Chung M-I, Flaherty DK, Matlock BK, Calvi CL, Blackwell TS, Ware LB, Bacchetta M, Walia R, Shaver CM, Kropski JA, McCarthy DJ, Banovich NE, Cell-type-specific and disease-associated expression quantitative trait loci in the human lung. *Nat. Genet* (2024), doi:10.1038/s41588-024-01702-0.
21. Salwig I, Spitznagel B, Vazquez-Armendariz AI, Khalooghi K, Guenther S, Herold S, Szibor M, Braun T, Bronchioalveolar stem cells are a main source for regeneration of distal lung epithelia in vivo. *EMBO J* 38 (2019), doi:10.15252/embj.2019102099.
22. Liu Q, Liu K, Cui G, Huang X, Yao S, Guo W, Qin Z, Li Y, Yang R, Pu W, Zhang L, He L, Zhao H, Yu W, Tang M, Tian X, Cai D, Nie Y, Hu S, Ren T, Qiao Z, Huang H, Zeng YA, Jing N, Peng

- G, Ji H, Zhou B, Lung regeneration by multipotent stem cells residing at the bronchioalveolar-duct junction. *Nat. Genet* 51, 728–738 (2019). [PubMed: 30778223]
23. Kim CFB, Jackson EL, Woolfenden AE, Lawrence S, Babar I, Vogel S, Crowley D, Bronson RT, Jacks T, Identification of bronchioalveolar stem cells in normal lung and lung cancer. *Cell* 121, 823–835 (2005). [PubMed: 15960971]
 24. Kimura S, Mutoh M, Hisamoto M, Saito H, Takahashi S, Asakura T, Ishii M, Nakamura Y, Iida J, Hase K, Iwanaga T, Airway M Cells Arise in the Lower Airway Due to RANKL Signaling and Reside in the Bronchiolar Epithelium Associated With iBALT in Murine Models of Respiratory Disease. *Front. Immunol* 10, 1323 (2019). [PubMed: 31244859]
 25. Huang Y, Kempen MB, Munck AB, Swagemakers S, Driegen S, Mahavadi P, Meijer D, van Ijcken W, van der Spek P, Grosveld F, Günther A, Tibboel D, Rottier RJ, Hypoxia-inducible factor 2 α plays a critical role in the formation of alveoli and surfactant. *Am. J. Respir. Cell Mol. Biol* 46, 224–232 (2012). [PubMed: 22298531]
 26. Burman A, Kropski JA, Calvi CL, Serezani AP, Pascoalino BD, Han W, Sherrill T, Gleaves L, Lawson WE, Young LR, Blackwell TS, Tanjore H, Localized hypoxia links ER stress to lung fibrosis through induction of C/EBP homologous protein. *JCI Insight* 3 (2018), doi:10.1172/jci.insight.99543.
 27. Mathieu JRR, Heinis M, Zumerle S, Delga S, Le Bon A, Peyssonnaud C, Investigating the real role of HIF-1 and HIF-2 in iron recycling by macrophages. *Haematologica* 99, e112–4 (2014). [PubMed: 24727819]
 28. Ratcliffe PJ, HIF-1 and HIF-2: working alone or together in hypoxia? *J. Clin. Invest* 117, 862–865 (2007). [PubMed: 17404612]
 29. Okubo T, Knoepfler PS, Eisenman RN, Hogan BLM, Nmyc plays an essential role during lung development as a dosage-sensitive regulator of progenitor cell proliferation and differentiation. *Development* 132, 1363–1374 (2005). [PubMed: 15716345]
 30. Degryse AL, Tanjore H, Xu XC, Polosukhin VV, Jones BR, McMahon FB, Gleaves LA, Blackwell TS, Lawson WE, Repetitive intratracheal bleomycin models several features of idiopathic pulmonary fibrosis. *Am. J. Physiol. Lung Cell. Mol. Physiol* 299, L442–52 (2010). [PubMed: 20562227]
 31. Mikami Y, Grubb BR, Rogers TD, Dang H, Asakura T, Kota P, Gilmore RC, Okuda K, Morton LC, Sun L, Chen G, Wykoff JA, Ehre C, Vilar J, van Heusden C, Livraghi-Butrico A, Gentsch M, Button B, Stutts MJ, Randell SH, O’Neal WK, Boucher RC, Chronic airway epithelial hypoxia exacerbates injury in muco-obstructive lung disease through mucus hyperconcentration. *Sci. Transl. Med* 15, eabo7728 (2023). [PubMed: 37285404]
 32. Russo PST, Ferreira GR, Cardozo LE, Bürger MC, Arias-Carrasco R, Maruyama SR, Hirata TDC, Lima DS, Passos FM, Fukutani KF, Lever M, Silva JS, Maracaja-Coutinho V, Nakaya HI, CEMiTool: a Bioconductor package for performing comprehensive modular co-expression analyses. *BMC Bioinformatics* 19, 56 (2018). [PubMed: 29458351]
 33. Hicks-Berthet J, Ning B, Federico A, Tilston-Lunel A, Matschulat A, Ai X, Lenburg ME, Beane J, Monti S, Varelas X, Yap/Taz inhibit goblet cell fate to maintain lung epithelial homeostasis. *Cell Rep* 36, 109347 (2021). [PubMed: 34260916]
 34. Kim W, Prokopenko D, Sakornsakolpat P, Hobbs BD, Lutz SM, Hokanson JE, Wain LV, Melbourne CA, Shrine N, Tobin MD, Silverman EK, Cho MH, Beaty TH, Genome-Wide Gene-by-Smoking Interaction Study of Chronic Obstructive Pulmonary Disease. *Am. J. Epidemiol* 190, 875–885 (2021). [PubMed: 33106845]
 35. Lee Y, Fryer JD, Kang H, Crespo-Barreto J, Bowman AB, Gao Y, Kahle JJ, Hong JS, Kheradmand F, Orr HT, Finegold MJ, Zoghbi HY, ATXN1 protein family and CIC regulate extracellular matrix remodeling and lung alveolarization. *Dev. Cell* 21, 746–757 (2011). [PubMed: 22014525]
 36. Polosukhin VV, Cates JM, Lawson WE, Milstone AP, Matafonov AG, Massion PP, Lee JW, Randell SH, Blackwell TS, Hypoxia-inducible factor-1 signalling promotes goblet cell hyperplasia in airway epithelium. *J. Pathol* 224, 203–211 (2011). [PubMed: 21557221]
 37. Liu K, Meng X, Liu Z, Tang M, Lv Z, Huang X, Jin H, Han X, Liu X, Pu W, Zhu H, Zhou B, Tracing the origin of alveolar stem cells in lung repair and regeneration. *Cell* 187, 2428–2445.e20 (2024). [PubMed: 38579712]

38. Aguilera KY, Brekken RA, Hypoxia Studies with Pimonidazole in vivo. *Bio Protoc* 4 (2014), doi:10.21769/bioprotoc.1254.
39. Wallace EM, Rizzi JP, Han G, Wehn PM, Cao Z, Du X, Cheng T, Czerwinski RM, Dixon DD, Goggin BS, Grina JA, Halfmann MM, Maddie MA, Olive SR, Schlachter ST, Tan H, Wang B, Wang K, Xie S, Xu R, Yang H, Josey JA, A Small-Molecule Antagonist of HIF2 α Is Efficacious in Preclinical Models of Renal Cell Carcinoma. *Cancer Res* 76, 5491–5500 (2016). [PubMed: 27635045]
40. Hu C-J, Poth JM, Zhang H, Flockton A, Laux A, Kumar S, McKeon B, Mouradian G, Li M, Riddle S, Pugliese SC, Brown RD, Wallace EM, Graham BB, Frid MG, Stenmark KR, Suppression of HIF2 signalling attenuates the initiation of hypoxia-induced pulmonary hypertension. *Eur. Respir. J* 54 (2019), doi:10.1183/13993003.00378-2019.
41. Wang F, Ting C, Riemondy KA, Douglas M, Foster K, Patel N, Kaku N, Linsalata A, Nemzek J, Varisco BM, Cohen E, Wilson JA, Riches DW, Redente EF, Toivola DM, Zhou X, Moore BB, Coulombe PA, Omary MB, Zemans RL, Regulation of epithelial transitional states in murine and human pulmonary fibrosis. *J. Clin. Invest* 133 (2023), doi:10.1172/JCI165612.
42. Katsura H, Sontake V, Tata A, Kobayashi Y, Edwards CE, Heaton BE, Konkimalla A, Asakura T, Mikami Y, Fritch EJ, Lee PJ, Heaton NS, Boucher RC, Randell SH, Baric RS, Tata PR, Human Lung Stem Cell-Based Alveolospheres Provide Insights into SARS-CoV-2-Mediated Interferon Responses and Pneumocyte Dysfunction. *Cell Stem Cell* 27, 890–904.e8 (2020). [PubMed: 33128895]
43. Van der Velden JL, Bertoncello I, McQualter JL, LysoTracker is a marker of differentiated alveolar type II cells. *Respir. Res* 14, 123 (2013). [PubMed: 24215602]
44. Sieber P, Schäfer A, Lieberherr R, Caimi SL, Lüthi U, Ryge J, Bergmann JH, Le Goff F, Stritt M, Blattmann P, Renault B, Rammelt P, Sempere B, Freti D, Studer R, White ES, Birker-Robaczewska M, Boucher M, Nayler O, NF- κ B drives epithelial-mesenchymal mechanisms of lung fibrosis in a translational lung cell model. *JCI Insight* 8 (2023), doi:10.1172/jci.insight.154719.
45. Wang S, Rao W, Hoffman A, Lin J, Li J, Lin T, Liew A-A, Vincent M, Mertens TCJ, Karmouty-Quintana H, Crum CP, Metersky ML, Schwartz DA, Davies PJA, Stephan C, Jyothula SSK, Sheshadri A, Suarez EE, Huang HJ, Engelhardt JF, Dickey BF, Parekh KR, McKeon FD, Xian W, Cloning a profibrotic stem cell variant in idiopathic pulmonary fibrosis. *Sci. Transl. Med* 15, eabp9528 (2023). [PubMed: 37099633]
46. Jaeger B, Schupp JC, Plappert L, Terwolbeck O, Artysh N, Kayser G, Engelhard P, Adams TS, Zweigerdt R, Kempf H, Lienenklaus S, Garrels W, Nazarenko I, Jonigk D, Wygrecka M, Klatt D, Schambach A, Kaminski N, Prasse A, Airway basal cells show a dedifferentiated KRT17^{high} phenotype and promote fibrosis in idiopathic pulmonary fibrosis. *Nat. Commun* 13, 5637 (2022). [PubMed: 36163190]
47. Usman S, Waseem NH, Nguyen TKN, Mohsin S, Jamal A, Teh M-T, Waseem A, Vimentin Is at the Heart of Epithelial Mesenchymal Transition (EMT) Mediated Metastasis. *Cancers* 13 (2021), doi:10.3390/cancers13194985.
48. Kidd ME, Shumaker DK, Ridge KM, The role of vimentin intermediate filaments in the progression of lung cancer. *Am. J. Respir. Cell Mol. Biol* 50, 1–6 (2014). [PubMed: 23980547]
49. Zheng D, Limmon GV, Yin L, Leung NHN, Yu H, Chow VTK, Chen J, A cellular pathway involved in Clara cell to alveolar type II cell differentiation after severe lung injury. *PLoS One* 8, e71028 (2013). [PubMed: 23940685]
50. Zuo W, Zhang T, Wu DZ, Guan SP, Liew A-A, Yamamoto Y, Wang X, Lim SJ, Vincent M, Lessard M, Crum CP, Xian W, McKeon F, p63(+)Krt5(+) distal airway stem cells are essential for lung regeneration. *Nature* 517, 616–620 (2015). [PubMed: 25383540]
51. Vaughan AE, Brumwell AN, Xi Y, Gotts JE, Brownfield DG, Treutlein B, Tan K, Tan V, Liu FC, Looney MR, Matthay MA, Rock JR, Chapman HA, Lineage-negative progenitors mobilize to regenerate lung epithelium after major injury. *Nature* 517, 621–625 (2015). [PubMed: 25533958]
52. Zacharias WJ, Frank DB, Zepp JA, Morley MP, Alkhaleel FA, Kong J, Zhou S, Cantu E, Morrisey EE, Regeneration of the lung alveolus by an evolutionarily conserved epithelial progenitor. *Nature* 555, 251–255 (2018). [PubMed: 29489752]

53. Yang Y, Riccio P, Schotsaert M, Mori M, Lu J, Lee D-K, García-Sastre A, Xu J, Cardoso WV, Spatial-Temporal Lineage Restrictions of Embryonic p63+ Progenitors Establish Distinct Stem Cell Pools in Adult Airways. *Dev. Cell* 44, 752–761.e4 (2018). [PubMed: 29587145]
54. Huang H, Fang Y, Jiang M, Zhang Y, Biermann J, Melms JC, Danielsson JA, Yang Y, Qiang L, Liu J, Zhou Y, Wang M, Hu Z, Wang TC, Saqi A, Sun J, Matsumoto I, Cardoso WV, Emala CW, Zhu J, Izar B, Mou H, Que J, Contribution of Trp63CreERT2-labeled cells to alveolar regeneration is independent of tuft cells. *Elife* 11 (2022), doi:10.7554/eLife.78217.
55. Kathiriya JJ, Brumwell AN, Jackson JR, Tang X, Chapman HA, Distinct Airway Epithelial Stem Cells Hide among Club Cells but Mobilize to Promote Alveolar Regeneration. *Cell Stem Cell* 26, 346–358.e4 (2020). [PubMed: 31978363]
56. Chen H, Matsumoto K, Brockway BL, Rackley CR, Liang J, Lee J-H, Jiang D, Noble PW, Randell SH, Kim CF, Stripp BR, Airway epithelial progenitors are region specific and show differential responses to bleomycin-induced lung injury. *Stem Cells* 30, 1948–1960 (2012). [PubMed: 22696116]
57. Ray S, Chiba N, Yao C, Guan X, McConnell AM, Brockway B, Que L, McQualter JL, Stripp BR, Rare SOX2+ Airway Progenitor Cells Generate KRT5+ Cells that Repopulate Damaged Alveolar Parenchyma following Influenza Virus Infection. *Stem Cell Reports* 7, 817–825 (2016). [PubMed: 27773701]
58. Choi J, Jang YJ, Dabrowska C, Iich E, Evans KV, Hall H, Janes SM, Simons BD, Koo B-K, Kim J, Lee J-H, Release of Notch activity coordinated by IL-1 β signalling confers differentiation plasticity of airway progenitors via Fosl2 during alveolar regeneration. *Nat. Cell Biol* 23, 953–966 (2021). [PubMed: 34475534]
59. Teisanu RM, Lagasse E, Whitesides JF, Stripp BR, Prospective isolation of bronchiolar stem cells based upon immunophenotypic and autofluorescence characteristics. *Stem Cells* 27, 612–622 (2009). [PubMed: 19056905]
60. Zheng D, Soh B-S, Yin L, Hu G, Chen Q, Choi H, Han J, Chow VTK, Chen J, Differentiation of Club Cells to Alveolar Epithelial Cells In Vitro. *Sci. Rep* 7, 41661 (2017). [PubMed: 28128362]
61. McClendon J, Jansing NL, Redente EF, Gandjeva A, Ito Y, Colgan SP, Ahmad A, Riches DWH, Chapman HA, Mason RJ, Tudor RM, Zemans RL, Hypoxia-Inducible Factor 1 α Signaling Promotes Repair of the Alveolar Epithelium after Acute Lung Injury. *Am. J. Pathol* 187, 1772–1786 (2017). [PubMed: 28618253]
62. Eckle T, Brodsky K, Bonney M, Packard T, Han J, Borchers CH, Mariani TJ, Kominsky DJ, Mittelbronn M, Eltzschig HK, HIF1A reduces acute lung injury by optimizing carbohydrate metabolism in the alveolar epithelium. *PLoS Biol* 11, e1001665 (2013). [PubMed: 24086109]
63. Vohwinkel CU, Burns N, Coit E, Yuan X, Vldar EK, Sul C, Schmidt EP, Carmeliet P, Stenmark K, Nozik ES, Tudor RM, Eltzschig HK, HIF1A-dependent induction of alveolar epithelial PFKFB3 dampens acute lung injury. *JCI Insight* 7 (2022), doi:10.1172/jci.insight.157855.
64. Yan Y, Liu F, Han L, Zhao L, Chen J, Olopade OI, He M, Wei M, HIF-2 α promotes conversion to a stem cell phenotype and induces chemoresistance in breast cancer cells by activating Wnt and Notch pathways. *J. Exp. Clin. Cancer Res* 37, 256 (2018). [PubMed: 30340507]
65. Torres-Capelli M, Marsboom G, Li QOY, Tello D, Rodriguez FM, Alonso T, Sanchez-Madrid F, García-Rio F, Ancochea J, Aragonés J, Role Of Hif2 α Oxygen Sensing Pathway In Bronchial Epithelial Club Cell Proliferation. *Sci. Rep* 6, 25357 (2016). [PubMed: 27150457]
66. Kathiriya JJ, Wang C, Zhou M, Brumwell A, Cassandras M, Le Saux CJ, Cohen M, Alysandratos K-D, Wang B, Wolters P, Matthay M, Kotton DN, Chapman HA, Peng T, Human alveolar type 2 epithelium transdifferentiates into metaplastic KRT5+ basal cells. *Nat. Cell Biol* 24, 10–23 (2022). [PubMed: 34969962]
67. Mohlin S, Wigerup C, Jögi A, Pählman S, Hypoxia, pseudohypoxia and cellular differentiation. *Exp. Cell Res* 356, 192–196 (2017). [PubMed: 28284840]
68. Brereton CJ, Yao L, Davies ER, Zhou Y, Vukmirovic M, Bell JA, Wang S, Ridley RA, Dean LSN, Andriotis OG, Conforti F, Brewitz L, Mohammed S, Wallis T, Tavassoli A, Ewing RM, Alzetani A, Marshall BG, Fletcher SV, Thurner PJ, Fabre A, Kaminski N, Richeldi L, Bhaskar A, Schofield CJ, Loxham M, Davies DE, Wang Y, Jones MG, Pseudohypoxic HIF pathway activation dysregulates collagen structure-function in human lung fibrosis. *Elife* 11 (2022), doi:10.7554/eLife.69348.

69. Copeland CA, Olenchock BA, Ziehr D, McGarrity S, Leahy K, Young JD, Loscalzo J, Oldham WM, MYC overrides HIF-1 α to regulate proliferating primary cell metabolism in hypoxia. *Elife* 12 (2023), doi:10.7554/eLife.82597.
70. Aquino-Gálvez A, González-Ávila G, Jiménez-Sánchez LL, Maldonado-Martínez HA, Cisneros J, Toscano-Marquez F, Castillejos-López M, Torres-Espíndola LM, Velázquez-Cruz R, Rodríguez VHO, Flores-Soto E, Solís-Chagoyán H, Cabello C, Zúñiga J, Romero Y, Dysregulated expression of hypoxia-inducible factors augments myofibroblasts differentiation in idiopathic pulmonary fibrosis. *Respir. Res* 20, 130 (2019). [PubMed: 31234835]
71. Chen L, Yang Y, Yan H, Peng X, Zou J, NEDD4L-induced β -catenin ubiquitination suppresses the formation and progression of interstitial pulmonary fibrosis via inhibiting the CTHRC1/HIF-1 α axis. *Int. J. Biol. Sci* 17, 3320–3330 (2021). [PubMed: 34512149]
72. Jeny F, Bernaudin J-F, Valeyre D, Kambouchner M, Pretolani M, Nunes H, Planès C, Besnard V, Hypoxia Promotes a Mixed Inflammatory-Fibrotic Macrophages Phenotype in Active Sarcoidosis. *Front. Immunol* 12, 719009 (2021). [PubMed: 34456926]
73. Ueno M, Maeno T, Nomura M, Aoyagi-Ikeda K, Matsui H, Hara K, Tanaka T, Iso T, Suga T, Kurabayashi M, Hypoxia-inducible factor-1 α mediates TGF- β -induced PAI-1 production in alveolar macrophages in pulmonary fibrosis. *Am. J. Physiol. Lung Cell. Mol. Physiol* 300, L740–52 (2011). [PubMed: 21239537]
74. Pullamsetti SS, Mamazhakypov A, Weissmann N, Seeger W, Savai R, Hypoxia-inducible factor signaling in pulmonary hypertension. *J. Clin. Invest* 130, 5638–5651 (2020). [PubMed: 32881714]
75. Okubo T, Hogan BLM, Hyperactive Wnt signaling changes the developmental potential of embryonic lung endoderm. *J. Biol* 3, 11 (2004). [PubMed: 15186480]
76. Degryse AL, Tanjore H, Xu XC, Polosukhin VV, Jones BR, Boomershine CS, Ortiz C, Sherrill TP, McMahon FB, Gleaves LA, Blackwell TS, Lawson WE, TGF β signaling in lung epithelium regulates bleomycin-induced alveolar injury and fibroblast recruitment. *Am. J. Physiol. Lung Cell. Mol. Physiol* 300, L887–97 (2011). [PubMed: 21441353]
77. Fleming SJ, Chaffin MD, Arduini A, Akkad A-D, Banks E, Marioni JC, Philippakis AA, Ellinor PT, Babadi M, Unsupervised removal of systematic background noise from droplet-based single-cell experiments using CellBender. *Nat. Methods*, 1–13 (2023). [PubMed: 36635552]
78. Korsunsky I, Millard N, Fan J, Slowikowski K, Zhang F, Wei K, Baglaenko Y, Brenner M, Loh P-R, Raychaudhuri S, Fast, sensitive and accurate integration of single-cell data with Harmony. *Nat. Methods* 16, 1289–1296 (2019). [PubMed: 31740819]
79. López Y, Nakai K, Patil A, HitPredict version 4: comprehensive reliability scoring of physical protein-protein interactions from more than 100 species. *Database* 2015 (2015), doi:10.1093/database/bav117.
80. La Manno G, Soldatov R, Zeisel A, Braun E, Hochgerner H, Petukhov V, Lidschreiber K, Kastriiti ME, Lönnerberg P, Furlan A, Fan J, Borm LE, Liu Z, van Bruggen D, Guo J, He X, Barker R, Sundström E, Castelo-Branco G, Cramer P, Adameyko I, Linnarsson S, Kharchenko PV, RNA velocity of single cells. *Nature* 560, 494–498 (2018). [PubMed: 30089906]
81. Bergen V, Lange M, Peidli S, Wolf FA, Theis FJ, Generalizing RNA velocity to transient cell states through dynamical modeling. *Nat. Biotechnol* 38, 1408–1414 (2020). [PubMed: 32747759]
82. Lange M, Bergen V, Klein M, Setty M, Reuter B, Bakhti M, Lickert H, Ansari M, Schniering J, Schiller HB, Pe'er D, Theis FJ, CellRank for directed single-cell fate mapping (2020).
83. Hsia CCW, Hyde DM, Ochs M, Weibel ER, ATS/ERS Joint Task Force on Quantitative Assessment of Lung Structure, An official research policy statement of the American Thoracic Society/European Respiratory Society: standards for quantitative assessment of lung structure. *Am. J. Respir. Crit. Care Med* 181, 394–418 (2010). [PubMed: 20130146]
84. Wegner KA, Keikhosravi A, Eliceiri KW, Vezina CM, Fluorescence of picosirius red multiplexed with immunohistochemistry for the quantitative assessment of collagen in tissue sections. *J. Histochem. Cytochem* 65, 479–490 (2017). [PubMed: 28692327]
85. Katsura H, Sontake V, Tata A, Kobayashi Y, Edwards CE, Heaton BE, Konkimalla A, Asakura T, Mikami Y, Fritch EJ, Lee PJ, Heaton NS, Boucher RC, Randell SH, Baric RS, Tata PR, Human Lung Stem Cell-Based Alveolospheres Provide Insights into SARS-CoV-2-Mediated Interferon

- Responses and Pneumocyte Dysfunction. *Cell Stem Cell* 27, 890–904.e8 (2020). [PubMed: 33128895]
86. Jacob A, Morley M, Hawkins F, McCauley KB, Jean JC, Heins H, Na C-L, Weaver TE, Vedaie M, Hurley K, Hinds A, Russo SJ, Kook S, Zacharias W, Ochs M, Traber K, Quinton LJ, Crane A, Davis BR, White FV, Wambach J, Whitsett JA, Cole FS, Morrisey EE, Guttentag SH, Beers MF, Kotton DN, Differentiation of Human Pluripotent Stem Cells into Functional Lung Alveolar Epithelial Cells. *Cell Stem Cell* 21, 472–488.e10 (2017). [PubMed: 28965766]
87. López Y, Nakai K, Patil A, HitPredict version 4: comprehensive reliability scoring of physical protein-protein interactions from more than 100 species. *Database* 2015 (2015), doi:10.1093/database/bav117.
88. Wallace EM, Rizzi JP, Han G, Wehn PM, Cao Z, Du X, Cheng T, Czerwinski RM, Dixon DD, Goggin BS, Grina JA, Halfmann MM, Maddie MA, Olive SR, Schlachter ST, Tan H, Wang B, Wang K, Xie S, Xu R, Yang H, Josey JA, A Small-Molecule Antagonist of HIF2 α Is Efficacious in Preclinical Models of Renal Cell Carcinoma. *Cancer Res* 76, 5491–5500 (2016). [PubMed: 27635045]
89. Bono H, Hirota K, Meta-Analysis of Hypoxic Transcriptomes from Public Databases. *Biomedicines* 8 (2020), doi:10.3390/biomedicines8010010

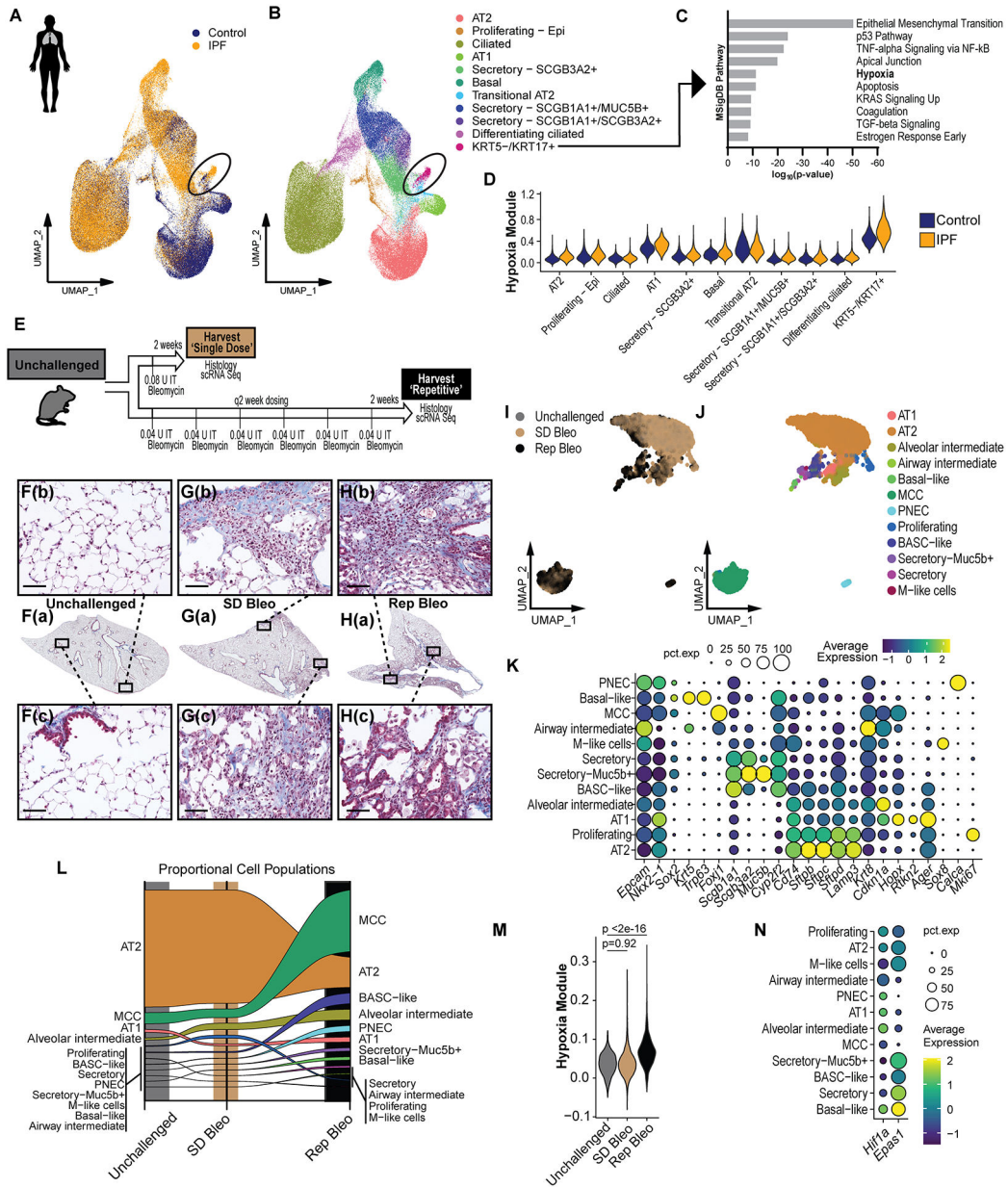


Figure 1. Recurrent injury leads to persistent activation of HIF-regulated programs in the lung epithelium.

(A and B) UMAP embedding of scRNA-seq of 194,132 epithelial cells from 67 PF and 49 control lungs from GSE227136 (20). Circle highlights disease-emergent KRT5⁻KRT17⁺ cells. (C) Pathway analysis of differentially expressed genes with Log₂-fold change >1 for KRT5⁻KRT17⁺ cells. (D) Hypoxia gene module score (calculated from genes extracted from ARCHs4 transcription factor analysis of HIF1A and EPAS1 of genes in (C) with statistically significant increase (p < 2 × 10¹⁶) pairwise Wilcoxon analysis adjusted for multiple comparisons). (E) Schematic of single-dose and repetitive intratracheal (IT) bleomycin mouse models. (F to H) Hematoxylin & Eosin (H&E) stains of representative lung sections from unchallenged mice (F) and mice following single-dose (SD Bleo, G) or repetitive IT bleomycin (Rep Bleo, H). Top images demonstrate overall architectural

changes. Center panels show whole lung slices. Bottom panels show representative epithelial changes. Scale bar = 50 μ m. (I and J) UMAP embedding of 6,583 cells from unchallenged, SD Bleo and Rep Bleo mice obtained following FACS-based Cd326⁺ enrichment and 10X 5' scRNA-seq. These data were jointly analyzed, embedded and annotated with other murine scRNA-seq (fig S1) for consistency across figures. (K) Dot plot of marker genes driving cell type annotation. (L) Alluvial plot showing proportional cell population changes between unchallenged, SD Bleo, and Rep Bleo mouse lungs, as determined by scRNA-seq. (M) Violin plot of Mouse MSigDB hypoxia module in mice (207 genes) across all epithelial cells from unchallenged, SD Bleo and Rep Bleo mice. Additional analysis by cell type is shown in fig. S2. (N) Dot plot of *Hif1* and *Epas1* expression across different cell clusters

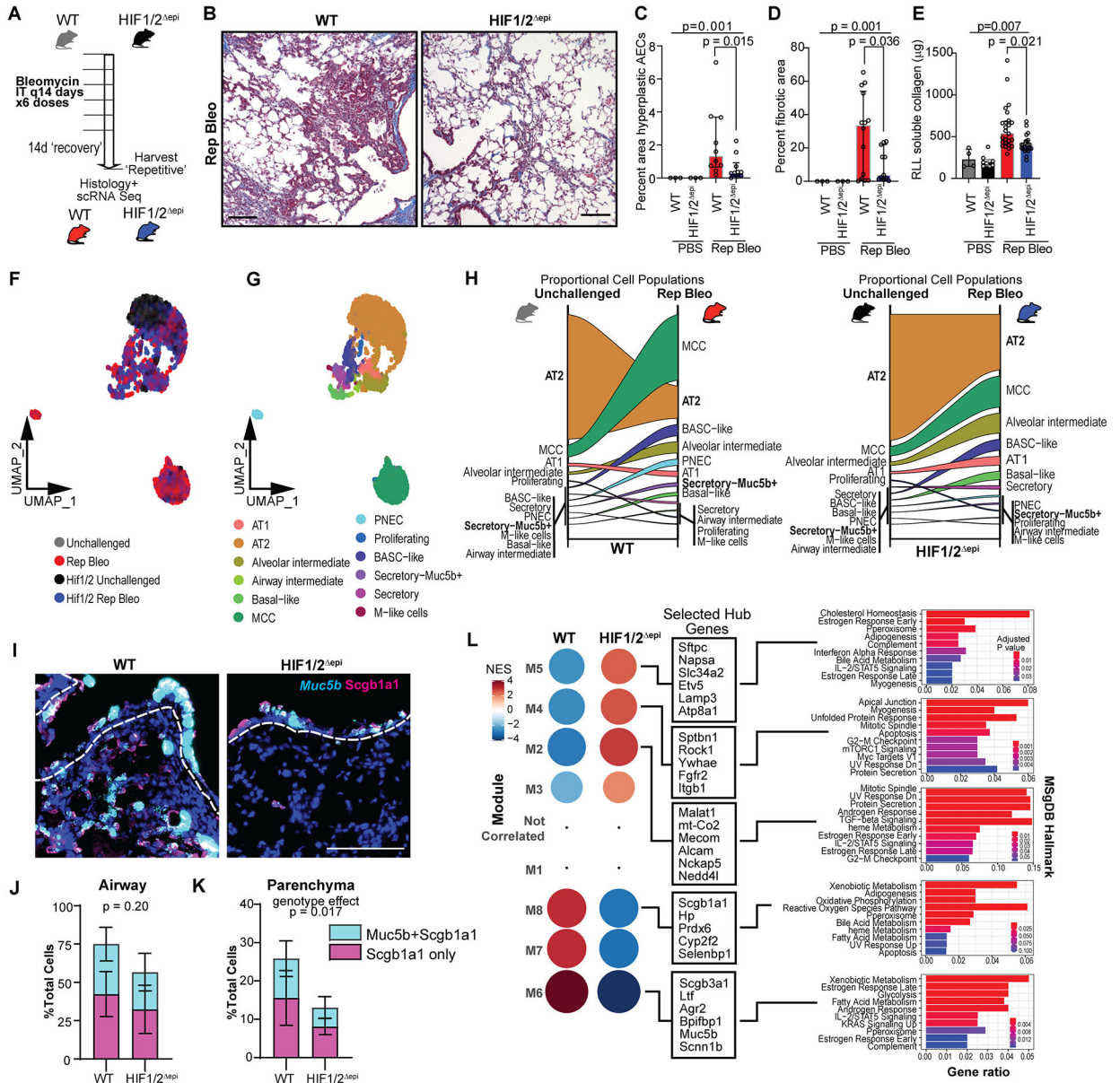


Figure 2. Epithelial deletion of *Hif1a* and *Epas1* modulates dynamics from recurrent injury and attenuates experimental fibrosis.

(A) Dosing and mouse genotype schematic of WT and *Hif1/2^{epi}* mice. (B) Masson Trichrome stained images of the different fibrotic responses modulated by combined epithelial *Hif1a* and *Epas1* deletion. Scale bar = 100µm. (C) Percent area per 20x field of hyperplastic epithelial cells. Plotted as median ±95% CI. (D) Histologic quantification of fibrotic area by masking. Plotted as median ±95% CI. (E) Collagen content (Sircol soluble assay) analysis of right lower lobe (RLL). Data plotted as median ±95% CI. (F) UMAP embedding of 5,105 sorted epithelial cells from WT and *Hif1/2^{epi}* mice showing genotype and treatment distribution. Data are pooled from N=3 mice per genotype and treatment condition. (G) UMAP of cell type annotation. Cells from *Hif1/2^{epi}* were embedded and jointly annotated (see fig. S1). Unchallenged and Rep Bleo WT mice are re-presented for

clarity across figures. (H) Alluvial plots of cell proportion comparing genotype and response to Rep Bleo. (I) RNA-ISH for *Muc5b* and IF of *Scgb1a1* from repetitive bleomycin treated *Hif1/2^{epi}* and control mice. Scale bar = 100 μm . (J and K) Quantitation of *Muc5b* and *Scgb1a1* cell proportion following Rep Bleo from 10 independent 40x fields across n=4 mice from each genotype. Airways masked for analysis. Plotted as mean \pm SD. Two-way analysis of variance (ANOVA) was performed, p-value reported from genotype contribution to variance. (L) Gene co-expression module enrichment analysis of the airway compartment (BASC, Secretory, Secretory-Muc5b⁺, Basal). Colored by Net enrichment (NES) and plotted by Z-score. Selected genes are presented from hubs within the modules and MSigDB pathway analysis of all module related genes. Table of gene modules, enrichment, top 30 gene hubs, and statistical analysis appears in Data file S1). Additional analysis of module enrichment per cell type and specific Protein-Protein interaction analysis appears in figs. S2 and S4).

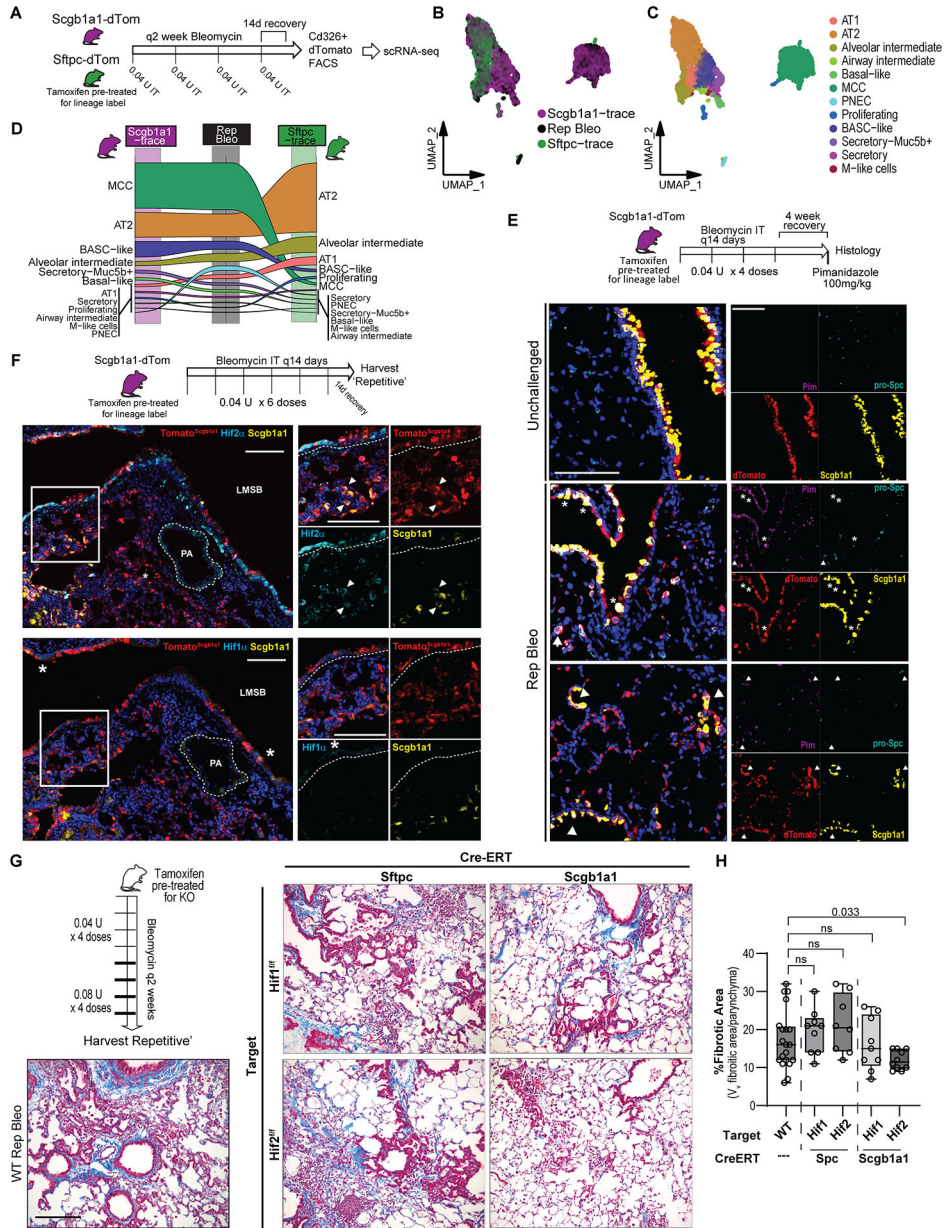


Figure 3. Airway-derived progenitors show Hif2-predominant activation in chronic injury. (A) Schematic for lineage-labeled *Sftpc*- or *Scgb1a1*-dTom mice with repetitive bleomycin injury and subsequent flow-cytometry based dTom⁺ sorting strategy for scRNA-seq. (B and C) UMAP embeddings of 7629 cells by lineage line and by cell type. (D) Alluvial plot comparing lineage-labeled (dTom⁺) cell proportions from *Scgb1a1*-traced (left) or *Sftpc*-traced (right) mice compared to total epithelial cells recovered from Rep Bleo injured mice. (E) Representative immunofluorescence images of *Scgb1a1*-traced Rep Bleo injured mice treated with Pimonidazole (Pim, 100 mg/kg) 2 hours prior harvest (detecting intracellular hypoxia or changed redox state, shown in magenta) colocalizing with tDtomato lineage-label (red), airway (*Scgb1a1*, yellow) and alveolar (pro-SPC, aqua) markers. Pim⁺dTom⁺ cells are annotated within the airway (*) and in the parenchyma (white arrowheads) with variable

Scgb1a1-protein staining. Scale bar = 100 μm . (F) Co-staining of Scgb1a1-lineage label with Hif1 or Hif2 using serial sections from Rep Bleo-injured mice. The top subpanel depicts an overview of the experimental design where Scgb1a1-lineage tracing mice were treated with tamoxifen followed by IT bleomycin every 2 weeks \times 6 cycles followed by sacrifice 14 days after the final bleomycin dose. The lower subpanels demonstrate immunofluorescence staining for Hif1 or Hif2 (each in aqua, top and bottom respectively) colocalized with tDtomato lineage label (red), and Scgb1a1 (yellow). White arrowheads indicate cells with nuclear (active) Hif2 in expanded region. (*) indicates Hif-positive cells of interest, for Hif1, cell showing Hif1⁺ are within the LMSB. Quantitation of nuclear (active) Hif1 and Hif2 is shown in fig. S4. LMSB = Left mainstem Bronchus, PA = Pulmonary artery. Scale bar = 100 μm . Additional data are shown in fig. S6A–D. (G) Fibrosis analysis from wild-type (WT), *Sftpc-CreER*; *Hif1a* or *Epas1* and *Scgb1a1-CreER*; *Hif1a* or *Epas1* conditional knockout mice subjected to repetitive bleomycin exposure. Schematic depicts the experimental design wherein WT and *Sftpc-CreER* or *Scgb1a1-CreER*, *Hif1a* or *Epas1* floxed mice were administered tamoxifen followed by a minimum 2-week washout then challenged with IT bleomycin every 2 weeks \times 8 cycles (0.04 IU/dose \times 4 cycles followed by 0.08 IU \times 4 cycles). Scale bar = 200 μm . (H) Fibrotic area of parenchyma was determined by quantification of Masson Trichome images. Detailed methodology can be found in the Supplementary Materials and Methods. Data are plotted as median with Min and Max whiskers. Following normality testing, a Welch ANOVA was used. ANOVA $p = 0.0024$, post-hoc comparisons only calculated for comparison to WT and depicted in the figure.

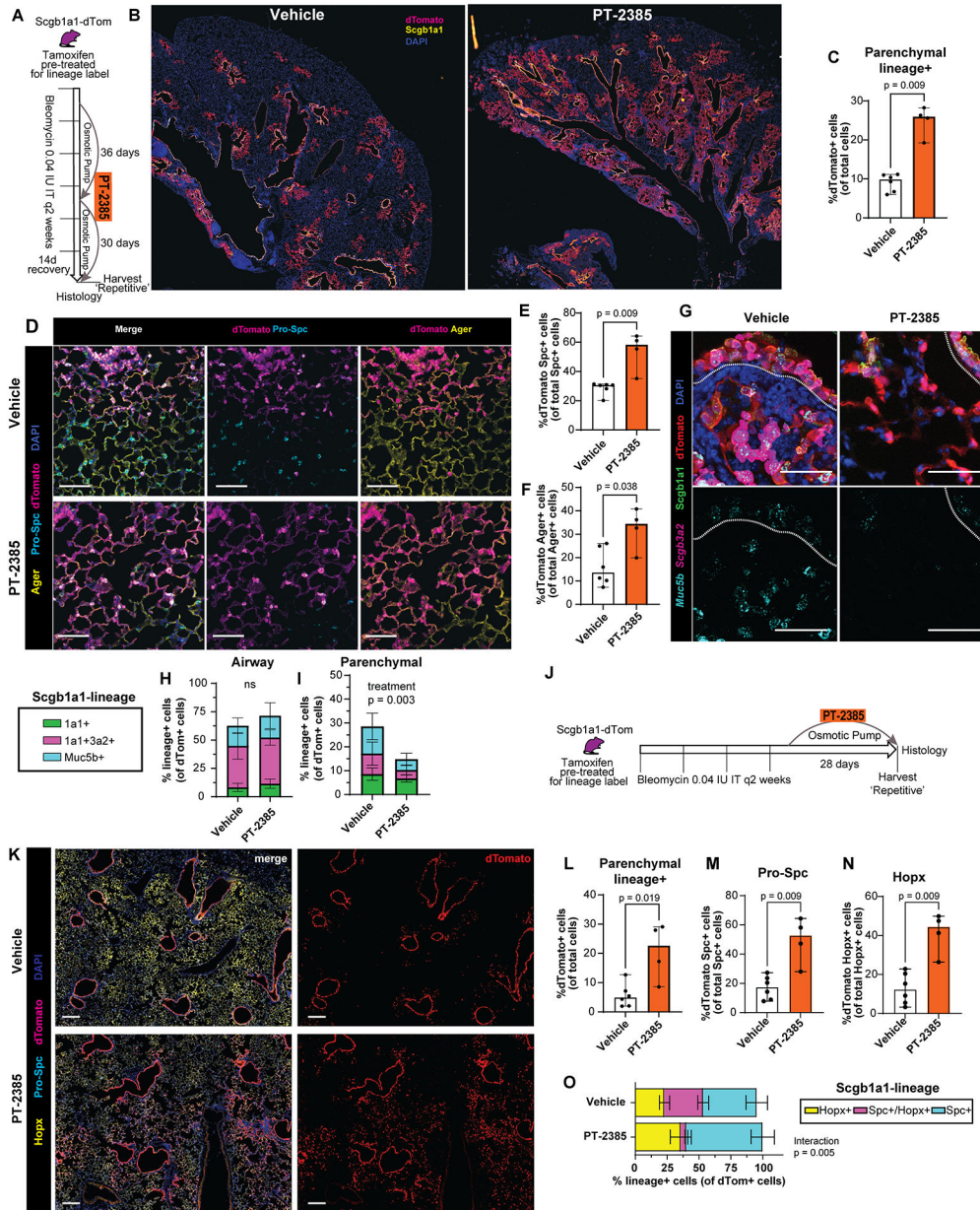


Figure 4. Pharmacologic inhibition of Hif2 enhances airway-derived adaptive epithelial repair following recurrent injury.

(A) Schematic of Rep Bleo in *Scgb1a1* lineage labeled mice with bi-weekly IT bleomycin. The Osmotic pumps containing PT-2385 (propylene glycol/DMSO vehicle) were implanted subcutaneously 1 week following the initial dose of bleomycin and were then replaced with fresh pumps following the fourth bleomycin administration. Mice were harvested for analysis two weeks following the sixth IT bleomycin dose. (B) Stitched images of *Scgb1a1*-lineage labeled cells in Vehicle vs PT-2385 from repetitive bleomycin treated mice. Scale bar = 1mm. dTomato = red, Scgb1a1 = yellow, (C) Quantification of dTomato⁺ *Scgb1a1*-lineage-derived cells outside airways. N=6 mice for control, N=4 for PT-2385 with at least 4 sections per mouse quantified. Plotted as median ±95% CI. (D) IF of pro-Spc (aqua), Ager (yellow), and *Scgb1a1*-lineage labeled dTomato (magenta). Scale bar = 50 μm.

(E and F) Quantification of pro-Spc (E) and Ager (F) with dTomato dual positivity. Two 5×5 stitched images were quantified per mouse comprising between 7900 to 15000 cells per field were quantified. Plotted as median ±95% CI. For F, Welch's test was used in accordance with a non-significant variance difference. (G) Combined RNA-ISH (*Muc5b* [aqua], and *Scgb3a2* [magenta]) and IF (*Scgb1a1* [green], dTomato [red]). Dotted line delineates the airway from adjacent parenchymal structures. Scale bar = 50 μm. (H and I) 10 separate images from N=6 vehicle and N=4 PT-2385 mice were masked to delineate airway (H) from parenchyma (I) and analyzed based on lineage and markers. Two-way ANOVA was performed. p-value reported from drug contribution to variance. (J) Schematic of 'rescue' treatment with PT-2385 after Rep Bleo in *Scgb1a1* lineage-labeled mice with bi-weekly IT bleomycin. The osmotic pumps containing PT-2385 (propylene glycol/DMSO vehicle) were implanted subcutaneously 1 week following the fourth dose of bleomycin and allowed to heal for a further 28 days before harvest. (K) Stitched 5×5 IF images of pro-Spc (aqua), Hopx (yellow), and *Scgb1a1*-lineage label dTomato (red). Scale bar = 200 μm. (L to N) Quantification of dTomato⁺ parenchymal cells as a percentage of total cells (L), pro-Spc (M), and Hopx with dTomato lineage label (N) as a fraction of the total marker pool (total Spc⁺-cells) after rescue treatment with PT-2385. N=6 control and N=4 PT-2385. Three 5×5 stitched images were quantified per mouse comprising between 36,883 and 58,213 total cells per mouse. Plotted as median ±95% CI. Mann Whitney U test. (O) Proportional outcome analysis of parenchymal *Scgb1a1* lineage-derived cells based on alveolar markers (pro-Spc and Hopx) as well as dual-positive cells. Plotted as mean±SD. Two way ANOVA was performed. P-value reported is for the interaction term between drug and cell proportion. Additional imaging of dual positive cells appears in fig. S6C.

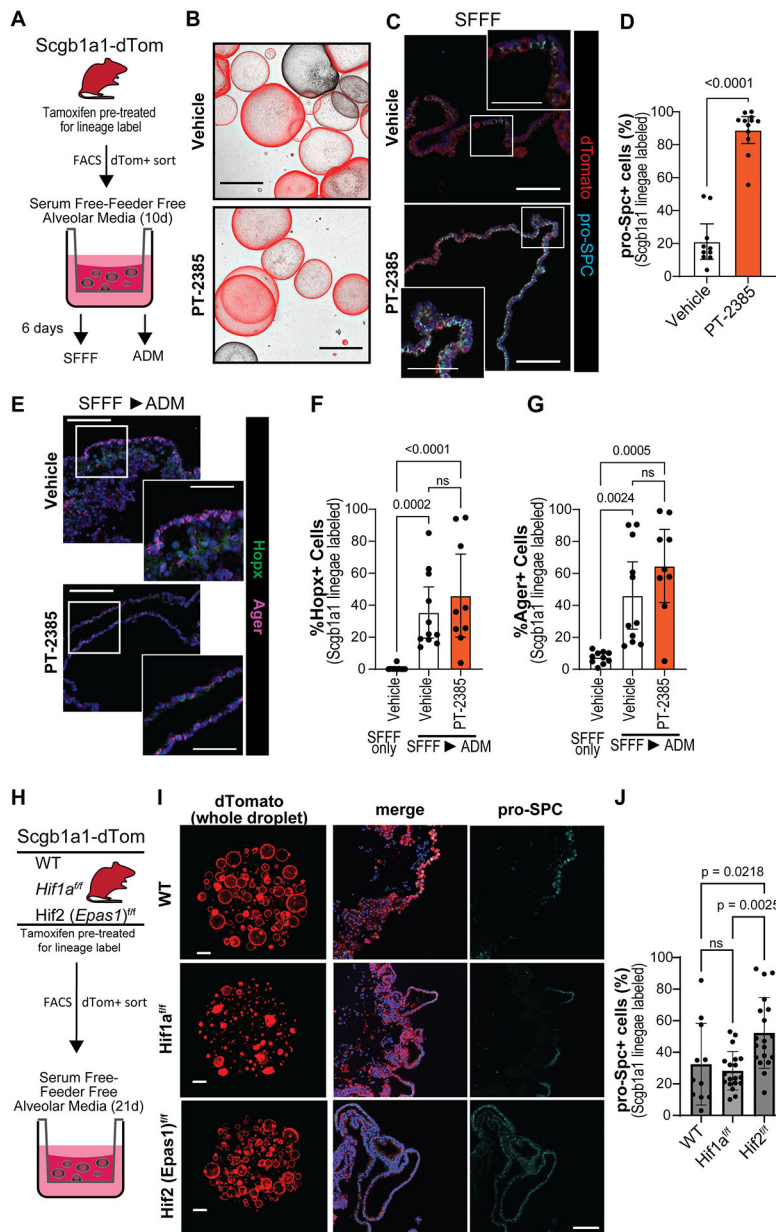


Figure 5. Inhibiting Hif2 promotes alveolar fate of airway-derived progenitors.

(A) Schematic of FACS sorting of *Scgb1a1*-lineage labeled cells for subsequent organoid culture derived from pooled cells from three mice. (B) Stitched overlay projection of brightfield and dTomato fluorescence of SFFF organoid outgrowth after 10 days. Scale bar = 1mm. (C) IF of organoids for pro-Spc (aqua) and dTom+ (red) cells. Scale bar = 100 μm, inset scale bar = 50 μm. (D) Quantification of pro-Spc+ *Scgb1a1*-lineage labeled cells per field of organoid, n=10 organoids per group across three technical replicate wells. (E) AT1-marker (Hopx [green], Ager [magenta]) staining of *Scgb1a1*-derived organoids after 7 days of SFFF expansion followed by transition to ADM for an additional 6 days. Scale bar = 100 μm, inset scale 50 μm. (F and G) Quantification of Hopx and Ager IF. Unique fields (comprising different organoids) spanning 2 technical replicates are displayed.

Kruskal-Wallis test, p-values reported for post-hoc comparisons with Dunn correction for multiple comparisons. (H) Schematic of FACS sorted of *Scgb1a1*-lineage labeled *Hif1a* or *Epas1* conditionally deleted cells for subsequent organoid culture derived from pooled cells from five mice. (I) Left column: Live whole-well fluorescent imaging of dTomato in respective droplets. Scale bar 1 mm. Center and right columns show IF of fixed organoids for pro-Spc and dTom⁺ cells. Scale bar = 100 μ m. Protein confirmation of knockout is shown in fig. S8. (J) Quantification of pro-Spc⁺ *Scgb1a1*-lineage labeled cells per field of organoid, 15 non-overlapping organoids per group across five technical replicate wells were imaged. Plotted as median \pm 95% CI. Kruskal-Wallis test, p values reported for post-hoc comparisons with Dunn correction for multiple comparisons.

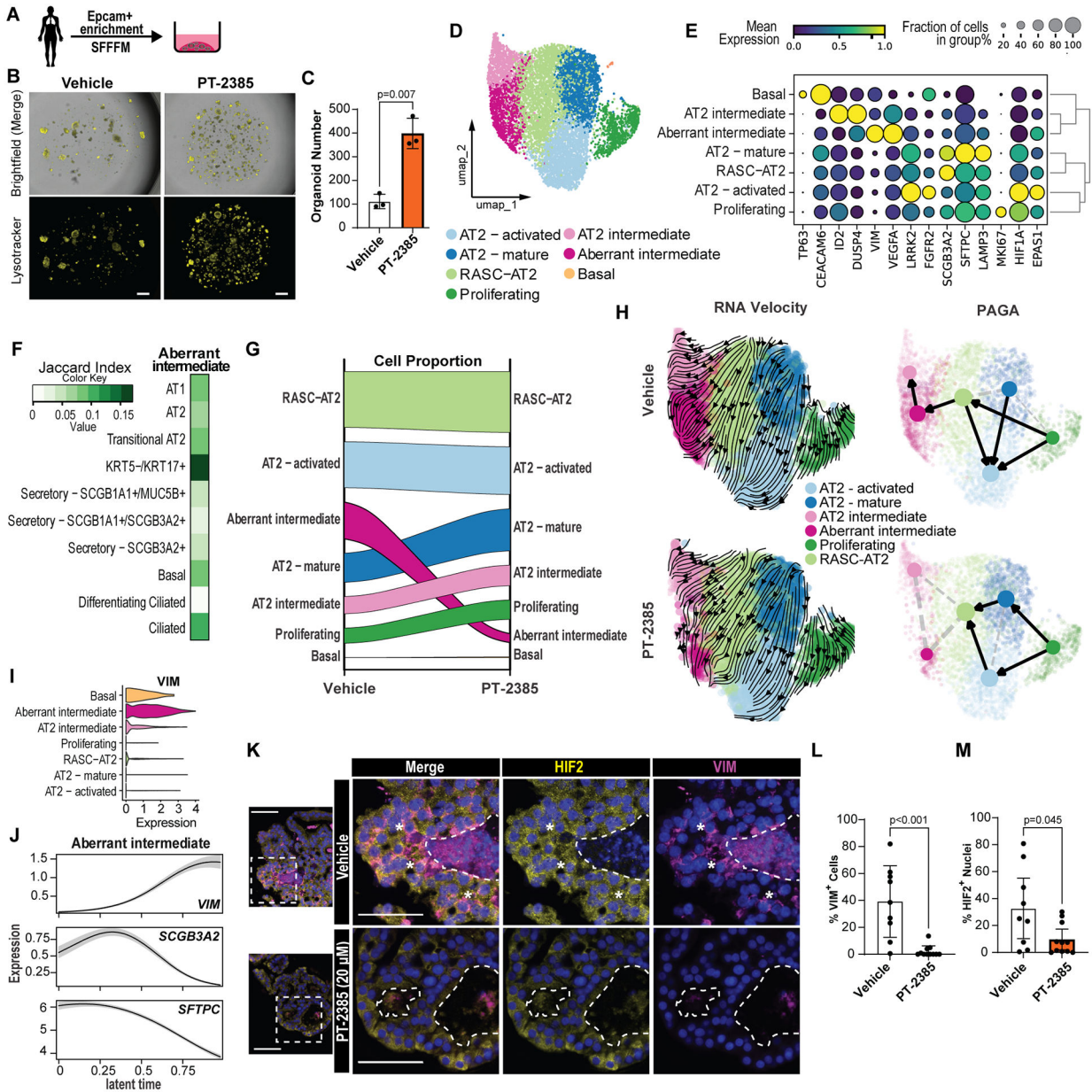


Figure 6. Inhibiting HIF2 enhances human alveolar organoid growth and prevents the emergence of aberrant intermediate cells. (A) Human organoid generation using declined donor tissue or ILD explants via CD326 enrichment and culture in SFFFM. (B) Brightfield and Lysotracker images of Vehicle and PT-2385-treated organoids (passage 1). Scale bar = 1mm. (C) Quantification of outgrowth from vehicle and PT-2385-treated organoids at 14d of passage 1. Analyzed with Welch’s t-test after ensuring variance did not significantly differ. (D) UMAP embedding of cell cluster annotation for 8694 cells across Vehicle (DMSO) and PT-2385 treatments. Treatment group embeddings appear in fig. S9. (E) Abbreviated dot plot for cluster annotation and marker gene expression. (F) Jaccard analysis of cluster-specific DE-genes ($\text{Log}_2\text{FC}>0.5$ and $p<0.001$) between the Aberrant intermediate cluster and full lung epithelial dataset shown in Fig. 1A. (G) Alluvial plot comparing cell proportions between Vehicle or PT-2385 (20 μM) -

treated organoids. (H) RNA velocity stream embeddings (left) and PAGA representations (right) for trajectory analyses of separately analyzed Vehicle and PT-2385 organoids demonstrating different dynamics between clusters, particularly within the RASC-AT2 cluster based on HIF2 inhibition. Further latent time embedding, differentially predicted terminal states and absorption probabilities appear in fig. S12 (I) Violin plot of *Vimentin* (*VIM*) expression across cell types. (J) Modeled *VIM*, *SCGB3A2*, and *SFTPC* marker gene expression along Cellrank-estimated latent time trajectory for Aberrant intermediate cells. (K) Representative IF of isolated organoids stained for Vimentin (magenta), HIF2 α (yellow) and their colocalization. Dotted lines delineate internal cavities of organoids for context. Asterisks indicate cells with both HIF2 α nuclear localization and cytoplasmic Vimentin. Scale bar = 50 μ m. (L and M) Quantification of Vimentin (L) and nuclear HIF2 α (M). 5 different organoids quantified across two technical replicates. Plotted as median \pm 95% CI.